



Review paper

Bio-soft matter derived from traditional Chinese medicine: Characterizations of hierarchical structure, assembly mechanism, and beyond



Guiya Yang^{a,1}, Yue Liu^{a,1}, Yuying Hu^a, Yue Yuan^c, Yunan Qin^d, Quan Li^{c,*},
Shuangcheng Ma^{a,b,**}

^a School of Traditional Chinese Medicine, Beijing University of Chinese Medicine, Beijing, 102488, China

^b Institute for Control of Chinese Traditional Medicine and Ethnic Medicine, National Institutes for Food and Drug Control, Beijing, 100050, China

^c Tianjin Key Laboratory of Therapeutic Substance of Traditional Chinese Medicine, School of Chinese Materia Medica, Tianjin University of Traditional Chinese Medicine, Tianjin, 301617, China

^d Collaborative Innovation Center for Advanced Organic Chemical Materials Co-constructed by the Province and Ministry, Ministry-of-Education Key Laboratory for the Synthesis and Application of Organic Functional Molecules, College of Chemistry and Chemical Engineering, Hubei University, Wuhan, 430062, China

ARTICLE INFO

Article history:

Received 2 October 2023

Received in revised form

3 January 2024

Accepted 31 January 2024

Available online 7 February 2024

Keywords:

Electron microscopy

Spectroscopy

Traditional Chinese medicine

Bio-soft matter

Structural characterization

ABSTRACT

Structural and functional explorations on bio-soft matter such as micelles, vesicles, nanoparticles, aggregates or polymers derived from traditional Chinese medicine (TCM) has emerged as a new topic in the field of TCM. The discovery of such cross-scaled bio-soft matter may provide a unique perspective for unraveling the new effective material basis of TCM as well as developing innovative medicine and biomaterials. Despite the rapid rise of TCM-derived bio-soft matter, their hierarchical structure and assembly mechanism must be unambiguously probed for a further in-depth understanding of their pharmacological activity. In this review, the current emerged TCM-derived bio-soft matter assembled from either small molecules or macromolecules is introduced, and particularly the unambiguous elucidation of their hierarchical structure and assembly mechanism with combined electron microscopic and spectroscopic techniques is depicted. The pros and cons of each technique are also discussed. The future challenges and perspective of TCM-derived bio-soft matter are outlined, particularly the requirement for their precise *in situ* structural determination is highlighted.

© 2024 The Author(s). Published by Elsevier B.V. on behalf of Xi'an Jiaotong University. This is an open access article under the CC BY-NC-ND license (<http://creativecommons.org/licenses/by-nc-nd/4.0/>).

1. Introduction

As a vital component of Chinese medicine and culture, traditional Chinese medicine (TCM) has made enormous contributions to healthcare, disease prevention and treatment [1]. Analysis of chemical constituents and elucidation of underlying pharmacological mechanisms constitute the long-term focus of modern pharmacology. Rapid advances in modern analytical techniques, particularly liquid chromatography and mass spectroscopy-based tools [2–4], guarantee fast and unambiguous molecular identification of various chemical constituents in TCM, thereby enabling rapid lead compound screening, solid quality evaluation, and TCM

regulation. The discovery of artemisinin from *Artemisia annua* L. (Qinghao) and its successful use in clinics, leading to the subsequent 2015 Nobel Prize in physiology and medicine, highlight the importance of TCM as the origin of new drug development [5].

Recent studies have revealed that many nanoassemblies, such as micelles, vesicles, particles, aggregates, and even gels, are formed during the preparation (e.g., decoction or processing) of TCM. Such bio-soft matters assembled from either a single chemical component or multiple components were found to exhibit different therapeutic effects compared to un-assembled or free molecules [6–8]. For example, the berberine (BBR) from *Coptis chinensis* Franch and rhein from *Rheum palmatum* L. were found to assemble into supramolecular nanoparticles, which demonstrate enhanced antibacterial activities compared with the individual BBR [9].

Currently, the discovery of these nanoscaled bio-soft matter has emerged as a new topic in the field of TCM. TCM-derived bio-soft matter refers to specific nano aggregates assembled from single or multiple bioactive components of TCM via non-covalent interactions.

* Corresponding author.

** Corresponding author. School of Traditional Chinese Medicine, Beijing University of Chinese Medicine, Beijing, 102488, China.

E-mail addresses: quanli85@tjctcm.edu.cn (Q. Li), masc@nifdc.org.cn (S. Ma).

¹ Both authors contributed equally to this work.

These aggregates differ significantly from unassembled individual components in terms of their pharmacological activities. The typical size of these aggregates ranges from 1 to 100 nm. Given the concept of modern soft matter science, pharmaceutically important macromolecules, such as polysaccharides and proteins found in TCM, are also indispensable members of TCM-derived bio-soft matter. The research of TCM-derived bio-soft matter attempts to explore and reveal the correlation between assembled structures and their bioactivities on the nanoscale. Instead of focusing on isolated bioactive molecules at the molecular level, the new concept of TCM-derived bio-soft matter does provide a unique perspective for unraveling the new effective form, namely the material basis of TCM at the level of supramolecular aggregates, further offering new opportunities for quality control over TCM on the nanoscale. The advantages of bio-soft matter derived from TCM lie primarily in their intrinsic bioactivity as well as their therapeutic potency as medications. Moreover, in the context of modern nanomedicine, the nanoscaled characteristics of such bio-soft matter may be utilized to improve the solubility, membrane permeability, and circulation, as well as the active targeting capabilities of herbal chemical components.

The TCM-derived bio-soft matter is usually formed “bottom-up” via the assembly of molecules with relatively weak and non-covalent interactions such as hydrogen bonds, π - π interactions, and hydrophobic interactions, among others [10,11]. Prior to investigating the pharmacological effects of such bio-soft matter, an unambiguous characterization of their hierarchical structures is required. Electron microscopy, which is the first choice to this end, has often been utilized to observe the morphology of bio-soft matter systems, as well as to measure their size and shape parameters. Additionally, extensive spectroscopy has to be utilized to reveal the nature of non-covalent interactions, the forces driving molecular assemblies, and the underlying mechanisms. The combined electron microscopic and spectroscopic characterizations of this bio-soft matter are obviously different from the traditional chromatography and mass spectroscopy-based analysis of the TCM components. Considering the fast rise of TCM-derived bio-soft matter, we believe it is time and necessary to summarize how to characterize the hierarchical structure of this type of bio-soft matter, particularly the utilities of electron microscopic and spectroscopic tools in their structural elucidation, further benefiting the eventual bio-evaluations. Thus, we first attempted to categorize the current TCM-derived bio-soft matter based on the molecular weight of the assembly units, comprising small molecules and macromolecules. Different subclasses of supramolecular aggregates, such as micelles, liposomes, vesicles, nanoparticles, and gels, have been identified, particularly in bio-soft matter assembled from small molecules. Here, we describe illustrative examples of TCM-derived bio-soft matter systems to demonstrate how combined electron microscopic and spectroscopic techniques may be used to accomplish unambiguous structural characterization of these systems and obtain a better understanding of the mechanisms underlying the assembly of these bio-soft matter systems. The advantages and disadvantages of each technique are discussed. By introducing emerging TCM-derived bio-soft matters, and elucidating their hierarchical structures via combined cross-scaled characterization techniques, we expect the prosperity of these bio-soft matter in the context of innovative medicine and biomaterial development would further contribute to personalized health care, diagnosis, and treatment, as advocated by TCM.

2. TCM-derived bio-soft matter assembled from small molecules

Many small molecules with self-assembling capabilities have been discovered in TCM [12]. Most of these molecules are

amphiphilic saponins that function as biosurfactants in medical and industrial applications. They have been found to self-assemble into diverse nanostructures, such as micelles, liposomes, vesicles, nanoparticles, and gels. In this section, we will focus on the usefulness of various structural characterization techniques aimed at gaining an understanding of the self-assembly of small molecules in TCM, as well as the role played by these techniques.

2.1. Micelles

Micelles are amphiphilic molecules that self-assemble into core-shell structures in selective solvent concentrations that are above the critical micelle concentration (CMC). This unique core-shell character endows the micelle with a useful “one-stone-two-birds” function, stemming from the water-soluble hydrophilic shell in bio-media and the hydrophobic core capable of carrying a cargo of drug molecules. Currently, molecular engineering of amphiphilic molecules has produced numerous scaffolds for building smart micelles, particularly those that are responsive to external stimuli, such as pH, light, and redox reactions, and are capable of delivering drug molecules to target locations.

In addition to synthetic amphiphile-based micelles, natural sources, particularly herb-derived small molecules that can self-assemble into micelles, have gained increasing attention in recent years owing to their intrinsic biocompatibility and therapeutic effects. Several molecules that can form micelles have been identified in herbal medicines. These small natural molecule-based micelles have been intensively studied from both fundamental and application points of view. However, an unambiguous understanding of the hierarchical structure of these biomicelles is essential for elucidating their structure-activity relationship at both the molecular and nanoscale levels. Hence, multiscale characterization of these nano-assemblies is often required.

Glycyrrhizic acid (GA) is a major herbal component isolated from the dried roots of *Glycyrrhiza uralensis* Fisch, *G. inflata* Bat. and *G. glabra* L. GA has been clinically developed as a hepatoprotective drug. Besides its anti-inflammatory and hepatoprotective functions, GA is reportedly capable of inhibiting various cancers. Interestingly, its amphiphilic structure (hydrophilic sugar moiety and hydrophobic triterpene backbone) enables GA to self-assemble into micelles in water at high concentrations (> 1 mM) and thereby serve as a drug delivery system [13]. In its capacity as a carrier material in drug delivery systems, GA shows a series of anti-cancer-related pharmacological activities, such as broad-spectrum anti-cancer activity, resistance to tissue toxicity caused by chemotherapy and radiation, drug absorption-enhancing effects, and anti-multidrug resistance mechanisms. Thus, novel GA-based drug delivery systems provide new opportunities for anticancer therapy. Yang et al. [14] prepared narrow and stable paclitaxel (PTX)-loaded GA micelles to improve the poor aqueous solubility and permeability of PTX. *In vitro* studies have shown that GA micelles may significantly improve the solubility of PTX (~200-fold increase). Characterization of the nanostructure of GA micelles via scanning electron microscopy (SEM) indicated that near-sphere micelles of PTX-loaded GA had been formed. GA micelles functioning as nanosized drug delivery systems allow drug permeation across the gastrointestinal barrier and resist uptake by the mononuclear phagocytic system [14]. As such, GA shows potential as a promising carrier for drug delivery via the oral route. Although SEM provides morphological information on micelles, the sample preparation and drying process involved may induce the formation of artifacts in the nanostructures. Moreover, microscopic observations may reveal only a selected area leading to a biased assessment of the overall morphology, thereby preventing an accurate representation

of the whole sample. Therefore, exploring the authentic micelle structure in the working environment, i.e., in the solution phase, would lead to more convincing results. Small-angle scattering (mainly small-angle X-ray or neutron scattering (SAXS) or (SANS)) is a powerful technique that can be used to probe nanostructures ranging from 1 to 300 nm in any state (solid, solution, gel, or gas). Readers may refer to classical textbooks and reviews on SAXS/SANS for details [15–19]. Using a combined power law and form factor $P(q)$ model fitting method, Matsuoka et al. [20] systematically studied the influence of pH and concentration on the self-assembling behavior of GA. The index value revealed that GA molecules in water at pH 5 or 6 could self-assemble into stable rod-like micelles. Based on this preliminary estimation of the GA assembly structure, model-dependent fitting was performed, resulting in a rod (cylinder) model being selected as the best fit (Fig. 1A) [20], thereby allowing the radius (~ 15 Å) and length (~ 210 Å) of the micelles to be obtained. Subsequently, Tucker et al. [21] systematically investigated the influence of electrolytes on the assembling behavior of GA in solution. They found that GA molecules self-assembled into elongated globular micelles at different concentrations ($c = 1$ – 5 mM). Experimental scattering data can be best fitted using a core-shell prolate ellipsoid model (Fig. 1B), which provides the dimensions of the inner core (R_1), containing the hydrophobic triterpene, and the outer shell (R_2), containing the saccharide groups of GA. SANS has been used to characterize the self-assembly properties of saponin GA. These results provide a sound basis for exploring a wider range of physicochemical

properties and help establish a wider portfolio of potential applications and interactions.

Gaining a better understanding of the underlying bottom-up mechanism leading to the formation of GA micelles, particularly the driving force produced by intermolecular interactions, is very important. To this end, molecular characterization based on spectroscopic or theoretical simulation is required. Matsuoka et al. [20] studied hydrophobic interactions between GA molecules in micelles using ^2H -nuclear magnetic resonance (NMR) spectroscopy and found that H–H interactions were extremely complex. Zelikman et al. [22] estimated the relatively stable structure of GA dimer units using molecular dynamics simulations. The results showed that the molecules in the dimer were quite close to each other and that there was no space between them into which another molecule (including the water molecule) could fit. Relatively stable dimer structures featuring specific angles between the terpene skeletons of the GA molecules and the sugar ends were found. Spontaneous transitions occur between these structures due to thermal motion. The insertion of a cholesterol molecule into the solution showed that, as a rule, the aggregates formed by two GA molecules and one cholesterol molecule yielded stable GA dimers with an attached cholesterol molecule. As indicated by many physicochemical studies and laboratory animal tests, the complexes formed between these pre-micellar GA aggregates and slightly soluble medicinal compounds were extremely stable and exerted the greatest therapeutic effect. It may be assumed that the effects observed in molecular dynamics simulations were linked to the increased solubility of medicinal compounds in GA complexes.

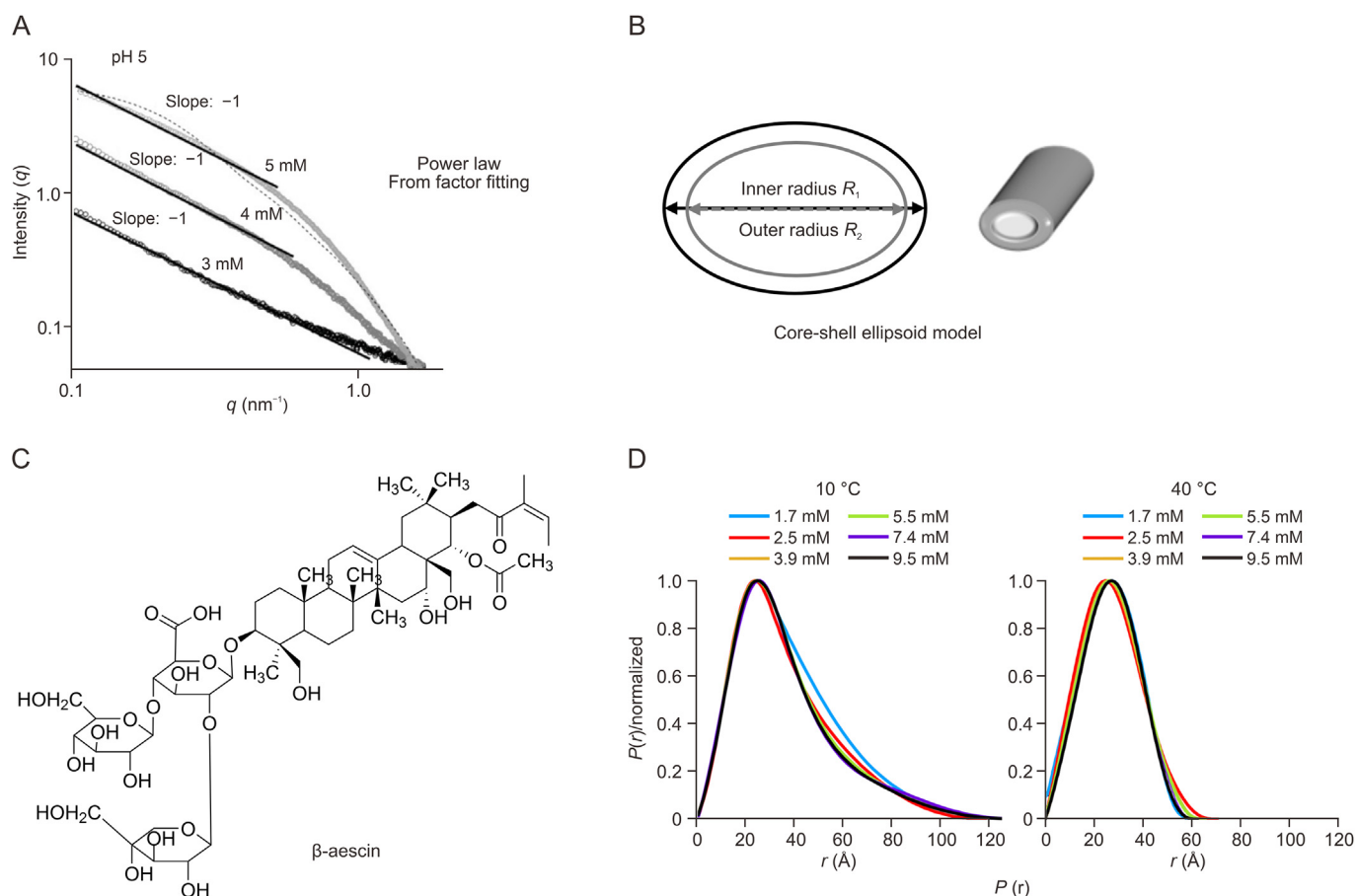


Fig. 1. (A) Small-angle X-ray scattering profiles with Power law and model fitting of glycyrrhizic acid micelle; (B) Core-shell ellipsoid model of glycyrrhizic acid micelle deduced from SasView program; (C) Chemical structure of β -aescin; (D) Pair distance distribution functions ($p(r)$) function of β -aescin with different concentrations at different temperatures. Reprinted from Refs. [20,23] with permission.

Besides GA molecules, aescin molecules (Fig. 1C) [23], extracted from the seeds of the horse chestnut tree, *Aesculus hippocastanum* (*Hippocastanaceae*), were also found to self-assemble into micelles. Hellweg and co-workers [23] used transmission electron microscopy (TEM) and SAXS to investigate the structure of aescin micelles. TEM indicated that these micelles, which exhibited a rod-like morphology, were accompanied by smaller and near-spherical objects. These smaller objects were assumed as having assembled into elongated rods because the number of spherical objects had decreased with increasing aescin concentration. They further investigated the temperature-dependent self-assembling properties of aescin micelles. They first determined the CMC at two different temperatures, where similar $CMC_{\text{aescin}}(10\text{ }^{\circ}\text{C}) = 0.38 \pm 0.09\text{ mM}$ and $CMC_{\text{aescin}}(50\text{ }^{\circ}\text{C}) = 0.32 \pm 0.13\text{ mM}$ were obtained at both temperatures, suggesting that CMC_{aescin} was not temperature-dependent within the experimental error range. To obtain the *in-situ* micelle structure in solution, SAXS was performed with different aescin concentrations at two different temperatures, which also provided concentration- and temperature-dependent structural information on the micelles. The scattering data were analyzed using the standard indirect Fourier transform (IFT) method, with the pair distance distribution functions ($p(r)$) indicating that the micelles possessed an elongated shape with a maximum size of roughly 120 Å for all concentrations measured at 10 °C. At a higher temperature (40 °C), the micelles exhibited a rather symmetrical shape, being either spherical or ellipsoidal, with a maximum size of 60–70 Å (Fig. 1D) [23]. Next, a model-dependent fitting method implemented in SasView was used to obtain more precise structural information on these micelles [23]. At 10 °C and 40 °C, the best fit to the experimental data was achieved with a cylinder model ($V_{\text{cylinder}} = \pi R^2 L$, where R and L are the radius and length of the cylinder, respectively) and an ellipsoid model ($V_{\text{ellipsoid}} = 4/3\pi R_p R_e^2$, where R_e and R_p are the equatorial and the polar radii of the ellipsoid, respectively) over a varying concentration range, respectively. The fit results at 10 °C suggested that the values of R (17–18 Å) and L (74–90 Å) for C_{aescin} remained almost unchanged between 1.7 and 9.5 mM. At a higher temperature, i.e., 40 °C, the cylindrical structure was transformed into an ellipsoid one, with the equatorial radius R_e remaining constant (~31 Å), and the polar radius R_p increasing slightly (13.2–16.8 Å) with increasing aescin concentration [23]. These results indicated that aescin micelles had undergone significant structural changes with increasing temperature, which were attributable to either changes in molecular packing or reductions in the forces between adjacent aescin molecules in the micellar structures. Potential triggers influencing the manner of packing may include the formation of hydrogen bonds between the polar groups of aescin molecules and hydration with water molecules. Herein, the monitoring of temperature- and concentration-dependent structural changes of the micelles highlighted the capability of SAXS that provide *in situ* structural information of the sample.

In addition to the abovementioned single-component-based micelles, herbal-derived mixed-component-based assemblies have been studied recently. Mixed-component-based assemblies are assumed to be more intriguing because diversity in molecular structure may allow individual components with diverse functions to be integrated into whole micelles. However, features of molecular structural diversity also pose challenges to any attempts at unambiguous characterization of the assembly mechanism and process. An interesting study of mixed-component-based assemblies was conducted by Thomas and co-workers [24]. SANS, another advanced scattering technique similar to SAXS, has been used to systematically study the self-assembly properties of several saponin mixtures, including escin/tea, tea/GA, and escin/GA, in solution. The structures of the assemblies of individual

components, particularly mixed binary components, could be quantitatively elucidated using a standard micelle core-shell model. These results provide interesting insights into factors regulating self-assembly in saponin-surfactant mixtures and the effects exerted on the self-assembly process by the saponin structure.

2.2. Liposome

Liposomes are spherical lipid vesicles (usually 50–500 nm in diameter) comprising one or more lipid bilayers. Liposomes show a high embedding rate for water- and lipid-soluble drugs and can be encapsulated in lipid-like membranes to form microvesicles. In recent years, liposomes have gained increasing attention owing to their potential for functioning as drug delivery systems that can effectively overcome the poor solubility of drugs, increase therapeutic efficiency, and reduce adverse events [25,26]. Interestingly, several liposomes with intrinsic bioactivities have also been found in TCM and used as drug carriers [27,28].

Ursolic acid (3 β -hydroxy-urs-12-en-28-oic acid, UA), a natural pentacyclic triterpene of the cyclosqualenoid family, has been isolated from various vegetarian foods, medicinal herbs, and plants. It modulates cellular transcription factors, growth factor receptors, inflammatory cytokines, and numerous other molecular targets, and regulates cell proliferation, metastasis, apoptosis, angiogenesis, and autophagy [29]. UA has long been considered a potentially valuable drug. Wang et al. [30] discovered that UA can form liposomes. Compared with the individual UA molecules, UA liposomes show more advantages, including favorable water solubility and bioavailability, passive targeting characteristics, and low toxicity [30]. Zhao et al. [31] chemically modified UA liposomes with water-soluble polyethylene glycol (PEG) and studied the physicochemical properties of liposome formulations, including encapsulation efficiency, particle morphology, size, stability, release rate *in vitro*, and cytotoxicity. Morphologically, conventional liposomes are nearly spherical with a size distribution in the 100–180 nm range. In comparison, the PEG-modified UA liposomes have a relatively uniform size distribution with diameters of 130–200 nm without contact or fusion phenomena. Atomic force microscopy (AFM) images of the UA liposomes showed similar sizes. AFM data demonstrated that these vesicles were regular spheres with a narrow size distribution range and good dispersity. The heights of the UA liposomes and PEG-modified UA liposomes were 52.2 nm and 163.2 nm, respectively. UA liposomes exhibit surface deformation and a middle sag. However, PEG-modified UA liposomes exhibited a more rigid structure, where strongly rigid liposomes presented a hemisphere with no intermediate concavity, while weakly rigid liposomes exhibited a concave pie shape. Compared with conventional liposomes, PEG-modified liposomes exhibited more rigidity and perfect morphology.

Geniposide (GE), the most abundant iridoid glucoside constituent of *Gardenia jasminoides* Ellis, exhibits excellent neuroprotective effects. However, GE has a short half-life and exhibits poor brain-targeting capabilities. To resolve these issues, Wan et al. [32] prepared a GE liposome-based drug delivery system aimed at treating cerebral ischemia-reperfusion injury. Characterization of GE liposomes, including particle size, zeta potential, and morphology, was conducted. The mean particle size of GE liposomes was 223.8 nm, while their polydispersity index was 0.159, indicating that the liposome particles had a narrow size distribution which enabled drugs to cross the blood-brain barrier and target brain cells. Their zeta potential was –6.17 mV, indicating that GE liposomes had a certain degree of stability. TEM revealed that GE liposomes had similar spherical or near-spherical shapes, without any apparent aggregation. The structural characterization of GE liposomes

showed that these liposomes had great potential for brain targeting. These self-assembling amphiphilic molecules which form liposomes may help resolve issues associated with poor water solubility and low bioavailability, thereby significantly improving therapeutic effects.

2.3. Vesicle

Vesicles are nanoscale membranous compartments formed by a lipid bilayer that separates their contents from the cytoplasmic or fluid-based extracellular environment. Vesicles are widely found in bacteria, animals, and plants. Lipid bilayers form the basic backbone of vesicles secreted by herbal plant cells. They encapsulate various proteins and active substances, such as nucleic acids, which play an important role in plant growth and development, tissue repair, and autologous defense processes. These plant vesicles have many advantages, such as low immune risk, few side effects, low production cost, and high safety profiles.

In addition to lipid molecules that form plant vesicles, several other bioactive molecules with amphiphilic characteristics have also been found to form vesicles. Saponins are plant-derived bio-surfactants. They have amphiphilic molecular structures, containing a hydrophobic triterpene or steroid aglycone and one or more hydrophilic sugar chains. Saponins are found in many herb plants, and many have been shown to promote the solubility of insoluble drugs [33,34]. Ginsenoside Ro (Ro), a natural anionic biosurfactant isolated from ginseng, the root of *Panax ginseng* C. A. Mey, has been found to increase the solubility of saikosaponin a (SSa) significantly. To gain an understanding of the mechanism through which Ro solubilizes Ssa, Dai et al. [35] investigated the self-assembly properties of Ro, Ssa, and mixed Ro/Ssa systems. TEM revealed that Ro self-assembled into spherical vesicles with diameters ranging from 30 to 50 nm. However, Ssa self-assembles into small spherical micelles which bind to each other to form large aggregates due to the strong hydrophobicity of Ssa molecules. Interestingly, when Ssa was added to the Ro solution, larger vesicles with diameters of 50–100 nm were formed, suggesting that Ssa had solubilized in the Ro vesicles to form mixed vesicles. Impressively, mesoscopic dynamics and dissipative particle dynamics simulations have been conducted in their research, and all the simulation results predicted well and were highly consistent with the experimental observations. This study, which deepens our understanding of the function of herbal plant saponins, may act as a guide for their application in the pharmaceutical industry. Xu et al. [36] also isolated vesicles from ginseng juice, termed G-Exos, which had a size of 144.1 ± 2.8 nm and a zeta potential of -27.4 ± 0.45 mV. SEM revealed that G-Exos was typically cup-shaped. Further studies indicated that G-Exos may efficiently stimulate the neural differentiation of bone marrow-derived mesenchymal stem cells (BMSCs) by transferring incorporated miRNAs to BMSCs. These results suggested that plant-derived vesicles may act as promising nanoplatfoms with much potential for use in neurodegenerative medicine.

For a more complicated self-assembly system, temperature-dependent bicelle-to-vesicle transition in mixtures of phospholipid 1,2-dimyristoyl-*sn*-glycero-3-phosphocholine (DMPC) and varied amounts of GA molecules in the presence of sucrose was investigated with the SAXS technique (Fig. 2A) [37]. Sucrose was employed to improve the contrast between the lipid membrane and the solvent. Model-independent IFT method was first used to predict the shape and dimension of the assemblies. It was revealed that the rate of heating from a low to a high temperature plays a vital role in vesicle formation. Heating rates of both 0.5 and 30 °C/min increased particle size as well as the GA ratio. A cylinder and core-shell sphere model from SasView was used to fit the experimental scattering data measured at 10 °C and 50 °C, respectively

(Fig. 2B) [37]. Several important size parameters, including cylinder radius (R_{cylinder}), cylinder height, equal to the thickness of the hydrophobic membrane part (H_{cylinder}), inner vesicle radius (R_{core}) and the thickness of the hydrophobic membrane part (t_{shell}), were evaluated using the fitting procedure. At a fixed temperature of 10 °C, R_{cylinder} was dependent on the amount of GA as indicated by R_{cylinder} decreasing with increasing GA ratio (Fig. 2C) [37]. For example, R_{cylinder} increased from 383.2 ± 28.2 at 35 mol% GA to 109.7 ± 3.5 at 70 mol% GA. Thus, the assembly behavior of mixed amphiphilic molecules demonstrated the possibility of preparing vesicles with a tailored structure, once the appropriate initial bicelle size, heating rate, and additives are selected. The shape, size, and polydispersity of the resulting structures are all can be investigated by SAXS. The results also highlight the power of SAXS for analyzing the multi-component assembly system derived from herbal medicines in the solution state.

2.4. Nanoparticles

In addition to the abovementioned self-assemblies (micelles, vesicles, and liposomes) with well-defined structures, many nanoparticles assembled via the bioactive components of TCM have also been discovered.

Using a solvent exchange method, Fan et al. [38] prepared UA nanoparticles, and fluorescein isothiocyanate (FITC)-labeled UA (FITC-UA) nanoparticles. UA nanoparticles with a size of 163.3 nm was finally obtained using an EtOH solution. The morphology of the UA nanoparticles was probed via TEM and AFM. These nanoparticles displayed monodispersed spherical shapes, indicating that good spherical shapes depend on stronger hydrophobic and hydrogen bonding interactions. X-ray diffraction (XRD) was used to investigate the molecular packing of UA in the nanoparticles. The solid UA sample exhibited sharp diffraction peaks with the 2 θ diffraction angles at 5.5, 8.38, 10.98, 14.9, 16.8, 22.01, and 27.12, suggesting the crystalline state of the solid sample. However, the UA nanoparticles exhibited only broad bands, indicating their amorphous state. The intermolecular interactions of UA were studied using ultraviolet-visible (UV-Vis) spectroscopy to unveil the driving force for self-assembly. The UV-Vis data showed that UA and FITC-UA nanoparticles were red-shifted compared to free UA molecules, indicating that the pentacyclic triterpenes may interact with each other via hydrophobic interactions. In addition, Wang et al. [39] investigated the self-assembly properties of six pentacyclic triterpenoids, including oleanolic acid (OA), UA, betulinic acid (BET), GA, liquidambaric acid (LA) and lupeol (Lup). All of these molecules were found to self-assemble into nanoparticles. A SEM based investigation of the morphologies of different nanoparticles indicated that OA and UA self-assembled into nanospheres, BET self-assembled into nanorods, GA self-assembled into nanosheets, and LA self-assembled into nanofibers, whereas nanoparticles formed by Lup constituted a mixture of nanospheres and nanofibers in a non-monolithic form (Fig. 3) [39]. These results showed that, although the chemical structures of the six pentacyclic triterpenoids were very similar, the assembly behaviors of these six were very different. Fourier transform infrared (FT-IR) spectroscopy was used to investigate intermolecular interactions between the compounds. The results showed that hydrogen bonding was the essential noncovalent intermolecular interaction that drove the assembly of pentacyclic triterpenoid molecules. Specifically, hydroxyl and carboxyl groups were involved in the formation of hydrogen bonds. Moreover, the hydrophobic interactions between the two molecular skeletons appear to differentiate the molecular assembly process, owing to the differences between molecular steric hindrances inherent in the triterpenoid skeleton. Computer simulations and various characterizations revealed the

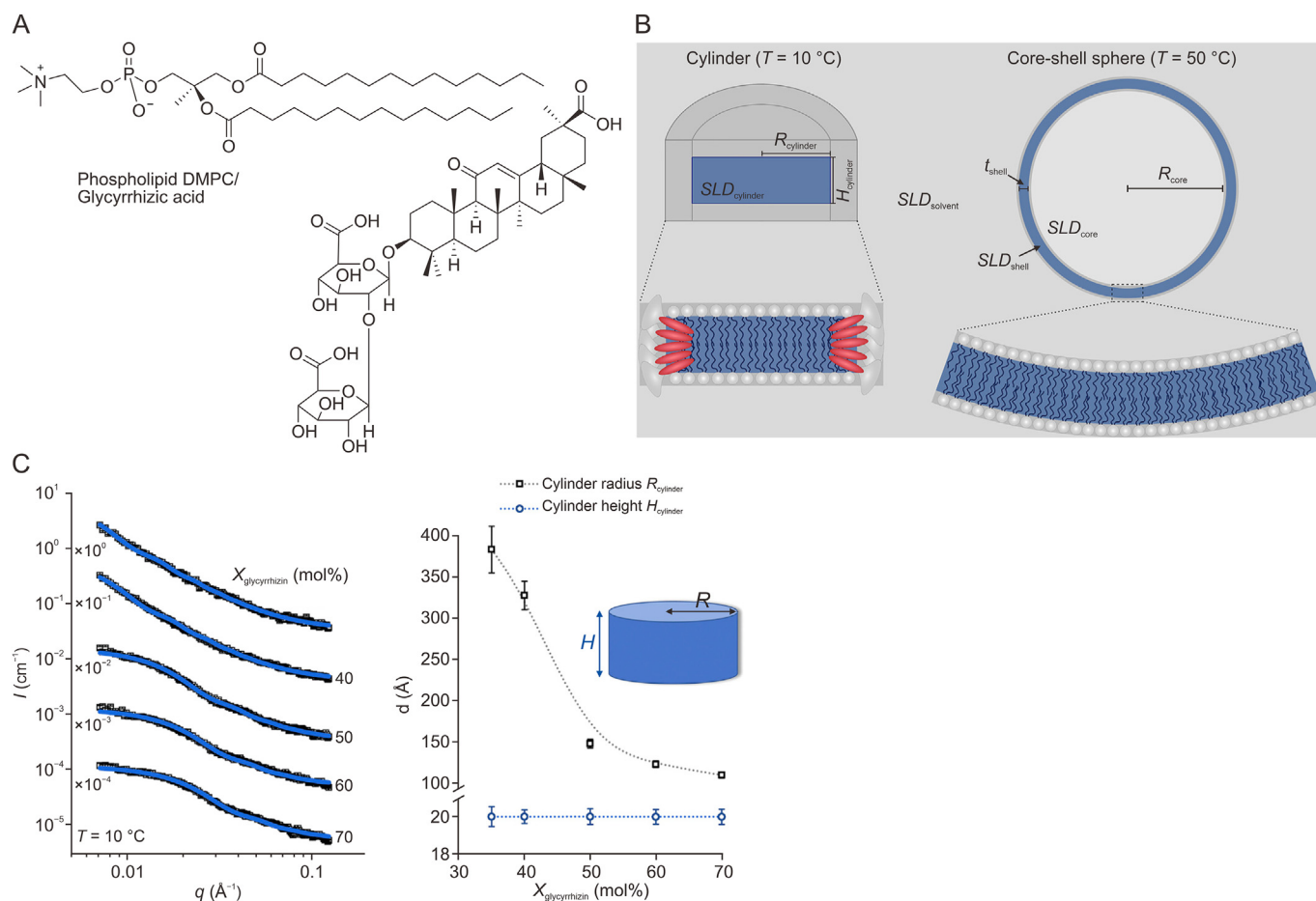


Fig. 2. (A) Chemical structures of phospholipid 1,2-dimyristoyl-*sn*-glycero-3-phosphocholine (DMPC)/glycyrrhizic acid. (B) Illustration of cylinder and core-shell sphere models for fitting the experimental small-angle X-ray scattering data using the SasView program. Left: At the temperature of $10\text{ }^{\circ}\text{C}$, the cylinder model is used to describe the bicellar shape, which is reduced to a cylindrical shape because of the contrast matching. Right: At the temperature of $50\text{ }^{\circ}\text{C}$, the core-shell sphere model is used to describe the vesicular shape.; (C) Left: SasView fitting of scattering data for DMPC/glycyrrhizic acid samples with varied glycyrrhizic acid molar ratios with cylinder model. Right: Changes of R_{cylinder} and H_{cylinder} with different glycyrrhizic acid ratios of DMPC/glycyrrhizic acid samples. Reprinted from Ref. [37] with permission.

mechanisms underlying the co-assembly of two small molecules. In brief, the nanoparticles constructed by a co-assembly strategy combine the advantages of “bioactivity” and “nano-system,” thereby offering a new perspective on the preparation of nanodrugs with pharmacological activity.

Compared with the single-component assembly system, in which only one herbal component exhibits self-assembly behavior, the multicomponent self-assembly system may be more robust because it enables such soft matter to achieve novel synergistic functions, resembling the macroscopic compatibility of different herbs in TCM, that individual components cannot achieve. Nevertheless, the presence of more components implies more complicated intermolecular interactions, multiple assembly pathways, and diverse assembly structures, all of which call for more precise structural characterization. BBR, an isoquinoline alkaloid isolated from the Chinese herb, *Coptis chinensis*, and other Berberis plants, exhibits excellent antibacterial activity. However, its application is limited due to low resistance. Wang and his team [6–9] found that BBR could self-assemble into well-defined nanostructures with several small molecules, such as rhein, cinnamic acid, and baicalin (BA), and that these nanostructures exhibited potent antibacterial activity. First, the microscopic morphologies of individual BBR, BA, and wogonoside (WOG) samples were observed via SEM. The morphology of BBR appeared as differently sized fragments or segments, while that of BA appeared as irregular sheets, and that of

WOG as long irregular strips, suggesting that the three small molecules did not self-assemble. Interestingly, after mixing BBR with BA and WOG at a certain ratio, a deepening of the solution color was observed, indicating that molecular self-assembly may have occurred in the solution. BBR was self-assembled into nanoparticles and nanofibers using BA and WOG, respectively. Field-emission scanning electron microscopy (FE-SEM) and TEM were used to investigate the micromorphologies of these self-assemblies (Fig. 4) [8]. Verification via a particle size analyzer indicated that the diameter of BA-BBR nanoparticles was approximately 100 nm. The self-assembled form of the WOG-BBR system was significantly different from that of the BA-BBR nanoparticles. Nanofiber bundles were observed using both FE-SEM and TEM. The diameters of these nanofibers were in the 50–100 nm range, while their lengths were in the tens of micrometers. UV-Vis, FT-IR, and fluorescence spectroscopies were employed to elucidate the intermolecular interactions involved and further deduce the mechanisms underlying molecular assembly. The UV-Vis absorption spectra of the BA-BBR nanoparticles, WOG-BBR nanofibers, and their individual monomers were measured at 200–500 nm (Fig. 5A) [8]. The characteristic absorption peaks ($\lambda_{\text{max}} = 273, 333\text{ nm}$) of BA-BBR nanoparticles contained the features of both BA ($\lambda_{\text{max}} = 276, 317\text{ nm}$) and BBR ($\lambda_{\text{max}} = 263, 345\text{ nm}$), suggesting that the complex consisted of BA and BBR units. Similar to the BA-BBR nanoparticles, the WOG-BBR nanofibers exhibited peaks characteristic

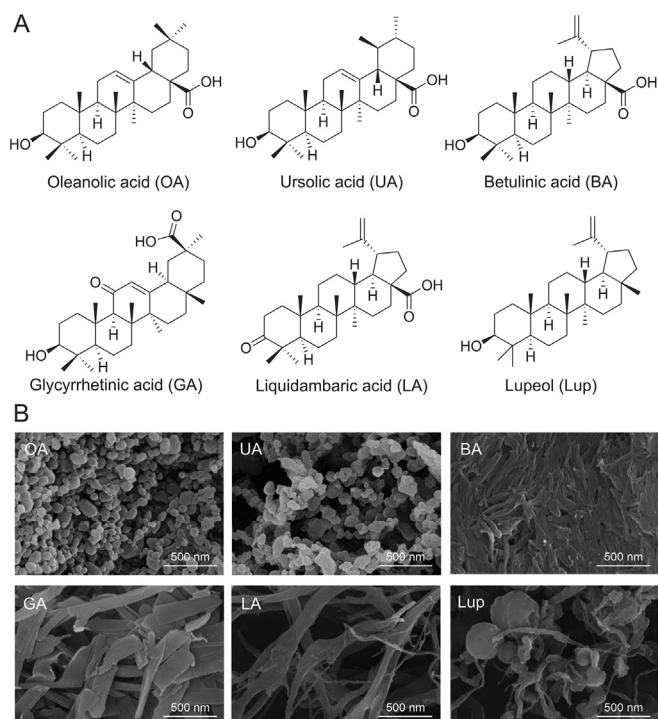


Fig. 3. (A) Structural formula of pentacyclic triterpenoids. (B) Scanning electron microscope images of self-assembled nanoparticles of pentacyclic triterpenoids. Reprinted from Ref. [39] with permission.

of their monomers. The binding sites of the BA-BBR and WOG-BBR complexes were investigated using FT-IR spectroscopy (Fig. 5B) [8]. The data showed that the peaks at 1726 cm^{-1} and 1746 cm^{-1}

corresponding to the stretching vibration of the carbonyl group on glucuronic acid of BA and WOG had shifted to a lower wavenumber (1615 and 1607 cm^{-1}) during self-assembly with BBR. This red-shift phenomenon may have been due to the electrostatic interaction between the carboxyl group and quaternary ammonium, leading to weak bond strength and slowed stretching vibration frequency of the C=O bond. Differences between the activities of BA-BBR nanoparticles and WOG-BBR nanofibers showed that different self-assembly morphologies may lead to different biological activities. Such studies may inspire the discovery and optimization of supramolecular self-delivering systems and provide opportunities for achieving optimal combinations of natural nanomedicines.

2.5. Supramolecular hydrogels

Supramolecular hydrogels, formed by noncovalent interactions among their constituent building units, have attracted attention due to their outstanding properties, including the tailorable synthesis of gelators, good biocompatibility, and biodegradability, particularly their dynamic feature in responsive to external stimuli such as pH, light, redox, and temperature [40–44]. These characteristics have enabled supramolecular hydrogels to be widely used in the fields of separation, adhesives, and actuators. These soft materials are used as smart biomaterials for purposes of drug delivery, tissue engineering, and wound healing [45]. Many molecules associated with TCM have been found to gel water and form supramolecular hydrogels [46–50]. These TCM-derived supramolecular hydrogel systems confer a distinct “one-stone-two-birds” advantage in that they can not only act as biomatrices or carriers but also perform diagnostic and therapeutic functions intrinsic to their bioactivity. Many gelators have been found in TCM, and their gels can be formed in various solvents [51]. Nevertheless,

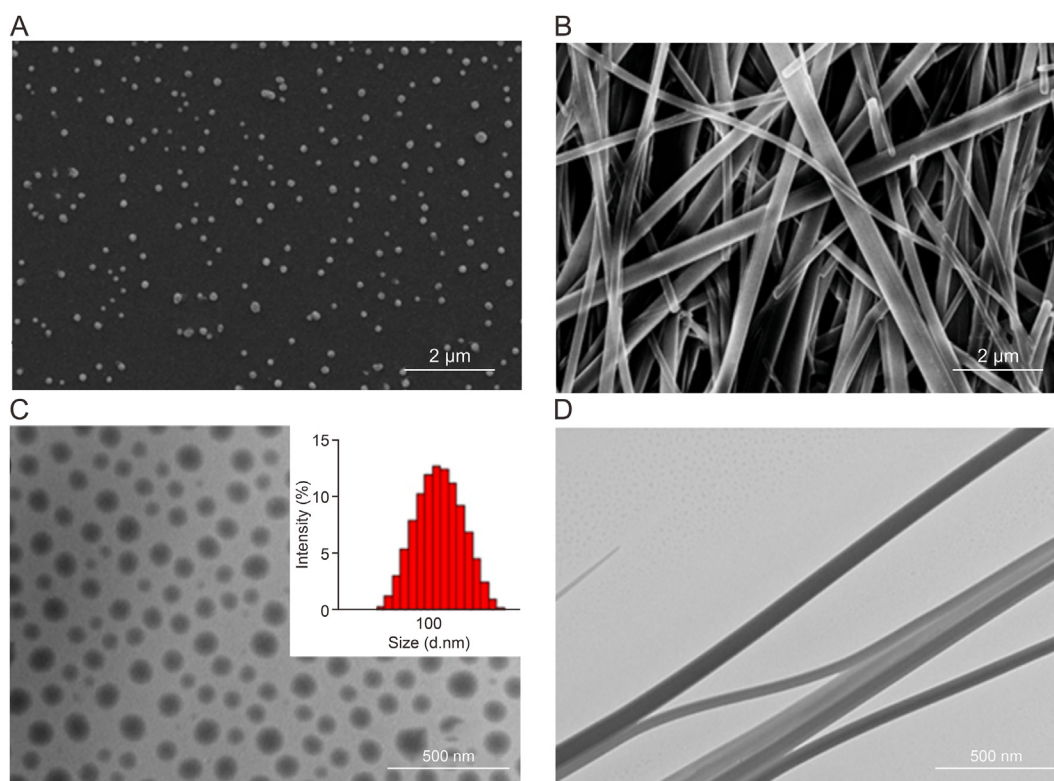


Fig. 4. Microscopic morphology of self-assemblies. (A, B) Scanning electron microscope images of 0.1 mM self-assemblies of baicalin (BA)-berberine (BBR) nanoparticles (A) and wogonoside (WOG)-berberine nanoparticles (B). (C, D) Transmission electron microscope images of 0.1 mM self-assemblies of baicalin-berberine nanoparticles (C) and wogonoside-berberine nanoparticles (D) (inset: particle size of baicalin-berberine nanoparticles). Reprinted from Ref. [8] with permission.

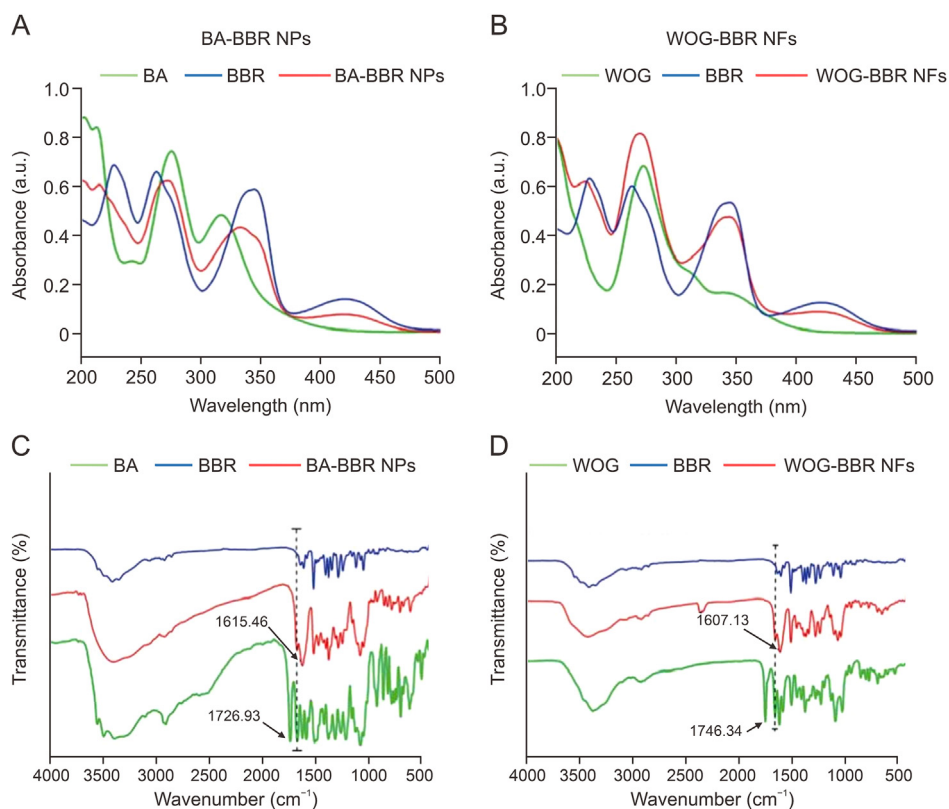


Fig. 5. Spectroscopic properties of self-assemblies. (A, B) Ultraviolet-visible spectroscopy of baicalin (BA)-berberine (BBR) nanoparticles (A) and wogonoside (WOG)-berberine nanofibers (B). (C, D) Fourier transform infrared spectrum of baicalin-berberine nanoparticles (C) and wogonoside-berberine nanofibers (D). Reprinted from Ref. [8] with permission.

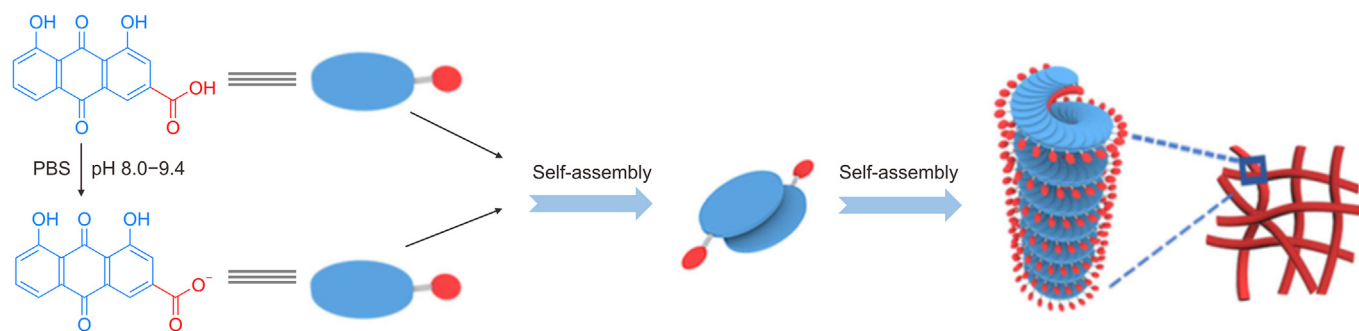


Fig. 6. Illustration of self-assembly process of the rhein hydrogel. Reprinted from Ref. [59] with permission.

considering the potential of these gels as biomedical applications, we herein include only hydrogelators that have an exceptional ability to gel water molecules.

Due to their hierarchical structural features, supramolecular hydrogels must be characterized using combined techniques that provide complementary information on different length scales. At the molecular scale (typically ≤ 2 nm), several spectroscopic methods, such as UV-Vis, fluorescence, FT-IR, and NMR, are frequently used to investigate non-covalent interactions (H-bond, π - π , CH- π , etc) driving the assembly of gelators. The strength of noncovalent interactions may also be probed using these spectroscopic methods via titration experiments. At the nanoscopic scale (typically 1–500 nm), the morphologies of gelator assemblies may be imaged via electron microscopy, including SEM, TEM, and AFM. SAXS is suitable for investigating such assembly structures in the wet state. To achieve the optimal functioning of biomedical

applications comprising supramolecular gels, their mechanical properties, such as elasticity or stiffness, should be adapted to the bioenvironment (skin, tissues, etc.). Hence, rheological characterization is often required to optimize the mechanical parameters of gels.

Many gelators discovered in TCM have been found to form supramolecular hydrogels. Puerarin (7,4'-dihydroxyisoflavone-8- β -D-glucopyranoside) is an isoflavone glycoside isolated from the root of the plant *Pueraria lobata*. It exhibits antioxidant properties, and reportedly exerts therapeutic effects on diseases, such as fevers [52], liver diseases [53], and cardiovascular diseases [54,55]. Cai et al. [56] reported that puerarin could self-assemble into a supramolecular hydrogel. Na₂CO₃ and HCl were added to different puerarin solutions ($c = 10, 20, \text{ and } 40$ mg/mL) in phosphate buffered saline (PBS) to adjust the pH, and subjected to a heating-cooling protocol to form the gel. The greater the concentration of

puerarin, the shorter the time required to form the hydrogel. Low puerarin concentrations (10 and 20 mg/mL) during gel preparation led to unstable hydrogel formation as well as crystal formation within the gels. However, high puerarin concentrations (40 mg/mL) resulted in the formation of stable hydrogels that showed good pH responsiveness in aqueous solutions. TEM was used to characterize the self-assembled nanostructures of the hydrogels. A typical nanofibrous structure could be observed via TEM. The hydrogels formed using higher concentrations of puerarin exhibited a dense fiber network, consisting of nanofibers characterized by larger diameters. The dense fiber network indicated that the gel possessed good mechanical properties and stability. Pang et al. [57] found that a hot puerarin solution gels water to form a hydrogel during cooling. SEM, which was used to visualize the gel network and characterize the morphology of puerarin hydrogels, indicated that a hydrogel was composed of an intertwined fibrous network containing internal pores that trapped water molecules via capillary action and surface tension. The pore size of the fibrous network of the hydrogel decreased as gelator concentration increased, indicating increased aggregation. NMR was used to explore the intermolecular interactions between puerarin molecules in order to determine the mechanism underlying the self-assembly of puerarin leading to the formation of hydrogel. Following gelation, all proton signals on the aromatic ring displayed a downfield shift, indicating that the puerarin molecule had undergone dramatic molecular self-assembly while transitioning from solution to gel state via $C=O-\pi$ interactions, because the electron-withdrawing group, $C=O$, on ring C reduces the shielding effect exerted by hydrogen on the aromatic rings (ring A and ring B). Changes in the 1H -NMR spectra corresponding to the transitioning from puerarin solution to gel suggested that $C=O-\pi$ interaction had triggered the self-assembly of puerarin molecules in water and initiated the gelation of puerarin hydrogel.

Another interesting natural hydrogelator is rhein, an anthraquinone compound isolated from TCM rhubarb. It self-assembles into hydrogels via non-covalent interactions, such as intermolecular $\pi-\pi$ interactions and hydrogen bonding, which can be characterized by fluorescence spectroscopy and XRD. Rhein hydrogels exhibit good solubility, slow release, low toxicity, and other responsive properties. Feng et al. [58] investigated the mechanism underlying the assembly of rhein and found that protonated rhein tends to aggregate, whereas deprotonated rhein self-assembles into spherical wormlike structures, forming a large number of discontinuous and highly dispersed states. Although these structures possess good thermodynamic solubility, they do not provide the required mechanical properties. Therefore, a rhodizone system only exists in an aqueous state. Zheng et al. [59] prepared rhein hydrogels in PBS using simple ultrasound and heating methods. The gel exhibited a uniform orange-red appearance [59]. SEM and TEM showed that the gels contained three-dimensional mesh-like structures composed of nanofibers. AFM and TEM showed that the average diameter of the nanofibers was approximately 30 nm, and that the length was a few micrometers. Further experiments indicated that the self-assembly process was strongly influenced by pH, with the optimal pH value being between 8.0 and 9.4, yielding a translucent hydrogel (Fig. 6) [59]. Zhao et al. [60] prepared a more complicated gel system, a supramolecular hydrogel containing self-assembled natural herbal rhein and a redox-responsive network based on ferrocene/ β -cyclodextrin host-guest recognition. This supramolecular network significantly improved encapsulation stability and maintained the structural integrity of self-assembled rhein, allowing its delivery to the wound site, thereby leading to better therapeutic effects. Other examples of self-assembling small molecules in TCM are summarized in Table 1 [61–80].

3. TCM-derived bio-soft matter assembled from macromolecules

In addition to small bioactive molecules, naturally-occurring biomacromolecules, such as polysaccharides and proteins, constitute another large family of natural products. Traditionally, macromolecules, such as polysaccharides and proteins, are assumed to be ineffective for purposes of TCM-based pharmaceutical preparation, and thus they were ignored or even discarded. However, recent studies have demonstrated that these macromolecules, which play important roles in healthcare and disease treatment, may be indispensable for TCM. Unlike small molecules with definitive bonds and structures, large molecules exhibit hierarchical structures on different length scales. For example, proteins demonstrate their structural hierarchy that being from amino acid constituent-sequence-linked primary structures to conformation/assembly-associated quaternary structures in space. The aggregation or entanglement of these biopolymer chains further complicates their subsequent structures, which eventually determine their micro- or macroscopic functions. Thus, the structural characterization of these biopolymers requires multiple spectroscopic and microscopic techniques.

3.1. Polysaccharides

Polysaccharides extracted from natural resources, such as plants, animals, and microorganisms, constitute a large family of biopolymers. Due to their excellent intrinsic biocompatibility and biodegradability, polysaccharides have been extensively developed for application in biomedical fields (drug delivery, 3D printing, excipients, etc.), as well as in cosmetic and food industries. Polysaccharide-based nanoparticles are known to improve the solubility of insoluble drugs, enhance their tissue-targeting ability, and facilitate the controlled and sustained release of drugs. A proper understanding of the hierarchical structures of these natural polysaccharides is vital for exploring their medicinal functions. For example, the molecular weight, monosaccharide composition, linking sequence, glycosidic linkage position, and conformation of polysaccharides must be unambiguously resolved prior to the elucidation of the structure-activity relationship. FT-IR spectroscopy may be used to identify monosaccharide types, glycosidic bonds, and functional groups, as well as to study intermolecular vibrations and polar bonds between different atoms. Compared to FT-IR spectroscopy, Raman spectroscopy can sensitively detect molecular vibrations and nonpolar bonds between the same atoms. NMR, an important tool that is used for analyzing the chemical structure of polysaccharides, primarily addresses the configuration of glycosidic bonds in polysaccharide structures and the number of monosaccharides in repetitive structures. Due to the rapid development of technologies such as 2D NMR, NMR has become a very powerful tool that is used to obtain structural information regarding polysaccharides.

In addition to the primary structure of polysaccharides, their higher-level structures, especially conformation, are essential for their bio-functions. Hence, conformational analysis of polysaccharides must be highly warranted. As a tool to observe the conformation of plant polysaccharide macromolecules, AFM can directly observe the conformation of individual macromolecules at the sub-nanometer scale and probe the intermolecular interactions of complex systems. Using AFM, Liang et al. [81] studied the conformation of glucomannogalactan, isolated from *P. geesteranus* fruiting bodies. Morphologies of undulating mountains (or islands) of varying sizes with heights of 10–100 nm and widths of 100–800 nm have been observed. Peak height may be regarded as a representation of chain length, which in turn reflects the lengths of

Table 1
Recent examples of traditional Chinese medicine (TCM)-derived bio-soft matter assembled from small molecules.

Assemblies	Compounds	Structural features	Characterization techniques	Ref.
Micelles	Ilex paraguariensis A. St. Hil saponins	Worm-like micelles	TEM	[61]
Micelles	Platycodin D	Spherical micelles with an average diameter of nearly 50 nm	TEM, DLS	[62]
Micelles	Baohuoside I	Spherical micelles	TEM	[63]
Liposome	Saikosaponin D	Spherical; smaller particle size (31.7 ± 7.8 nm)	TEM	[64]
Liposome	Baicalin	Spherical or elliptical; mean particle size of 87.6 ± 1.6 nm	cryo-TEM, DLS	[65]
Liposome	Ginger	Spherical; an average hydrodynamic diameter of ~ 188.5 nm; lower polydispersity	TEM, AFM, and DLS	[66]
Vesicle	Ginger	Elliptical and spherical vesicles; size with 206.8 ± 81.1 nm	TEM, DLS	[67]
Vesicle	Garlic	Spherical and irregular vesicle; the mean particle size 200 nm	TEM, DLS	[68]
Vesicle	Mulberry bark	A sphere having a bimolecular structure; average diameter of 151.3 ± 45.4 nm	TEM, DLS	[69]
Vesicle	Oleanolic acid	Spherical shape	TEM	[70]
Nanoparticles	Ivy	Uniform and spheroidal ivy nanoparticles; size ~ 100 nm	AFM, DLS	[71]
Nanoparticles	Chinese Yam	Polydisperse systems; many particles have diameters of around 200 nm, and others are larger or aggregated	AFM	[72]
Nanoparticles	Oleanolic acid	Regular spheres; size < 200 nm	SEM, DLS	[73]
Nanoparticles	Glycyrrhetic acid	Slab-like shape; size > 800 nm	SEM, DLS	[73]
Nanoparticles	Betulinol	Fibers; size > 800 nm	SEM, DLS	[73]
Nanoparticles	Betulonic acid	Fibers; size > 600 nm	SEM, DLS	[74]
Nanoparticles	Abietic acid	Uniform spheres; size between 258 and 289 nm	SEM, DLS	[75]
Hydrogels	Glycyrrhizic acid	Thin layers	AFM	[76]
Hydrogels	Betulonic acid	Fibers; size between 10 and 12 nm; Fibers; size between 40 and 50 nm	SEM, AFM	[77]
Hydrogels	Betulin	Flower-like objects; size between 200 and 1000 nm	FESEM, DLS	[78]
Hydrogels	Poricoic acid A	Fibrous gel	SEM, TEM	[79]
Hydrogels	Dehydrotumulosic acid	Fibrous gel	SEM, TEM	[79]
Hydrogels	liquidambaric acid	Fibrous gel	SEM, TEM	[79]
Hydrogels	Ursolic acid	Layered structures	SEM	[80]

Note: TEM: transmission electron microscope; DLS: dynamic light scattering; AFM: atomic force microscopy; SEM: scanning electron microscope; FESEM: field-emission scanning electron microscopy.

branched chains. Peak width reflects the intermolecular aggregation behavior of the molecules. AFM indicated that glucomannogalactan has long branched chains or stacked multilayers and displays molecular aggregation to some extent. Yuan et al. [82] used AFM to investigate the morphology of heteropolysaccharides isolated from *Angelica sinensis*. They observed many irregular spherical clusters with an average height of 10.5 nm. This value was higher than the average height of single polysaccharide chains, indicating the presence of branched chains and entanglement between the polysaccharides. SAXS is also a powerful tool that can be utilized to elucidate the structure of polysaccharides. The earliest work in this field was conducted by Kratky et al. [83]. Based on a plot of scattering data ($lq^2 \sim q$, Kratky plot) on cellulose nitrate, the persistence length (l_p) of the polymer was deduced, allowing the coiling degree of the polymers to be directly evaluated. Thanh and his team [84–86]

extracted several fucoidans with antimicrobial and intestinal immunomodulatory activities from brown seaweed species (Fig. 7A) [84]. The conformational structures of these polysaccharides were probed using SAXS and molecular modeling. The cross-sectional Guinier plots indicated a bulky chain conformation for fucoidan (Fig. 7B) [84]. Notably, based on the obtained chemical structures, a series of molecular models were built, and the theoretical scattering curves of these molecular models were calculated and compared with the experimental SAXS curves (Fig. 7C) [84]. To date, fully characterizing the structure of polysaccharides, particularly their chain conformation, remains challenging. Nevertheless, this “trial-and-match” method highlights the possibility of accessing the most approximate or even precise chain structure of polysaccharides. Typical examples of the nanostructural characterization of polysaccharides from TCM are summarized (Table 2) [87–102].

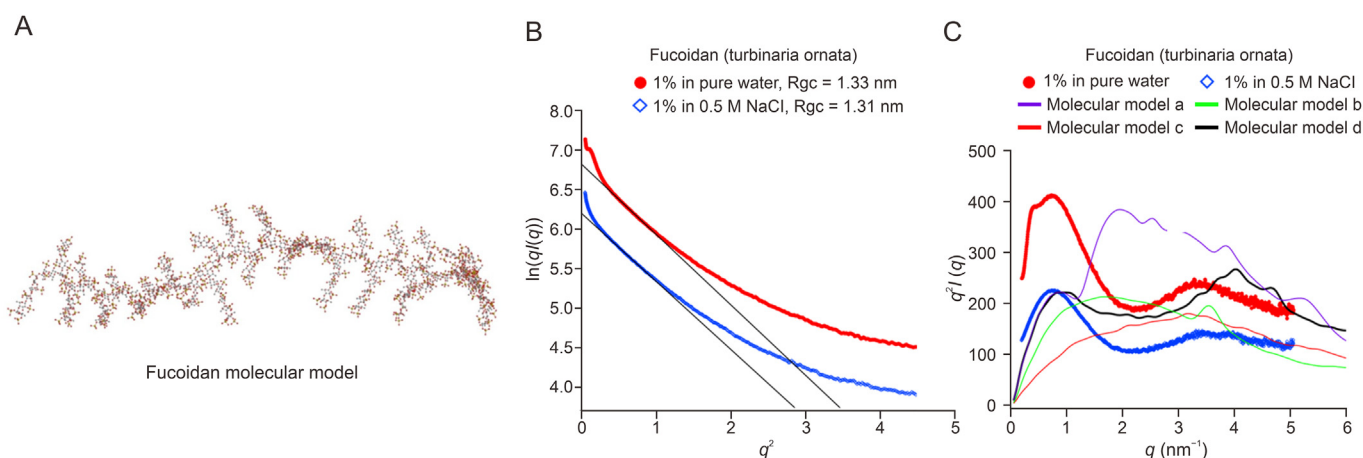


Fig. 7. (A) Molecular model of fucoidan. (B, C) Small-angle X-ray scattering profiles of fucoidan with cross-section Guinier plots (B) and Kratky plots (C). Reprinted from Ref. [84] with permission.

Table 2
Nanostructural characterization of polysaccharides from traditional Chinese medicine (TCM).

Compounds	Structural features	Characterization techniques	Ref.
Jujube polysaccharides	Thin slice; spherical; fibers; spherical lumps; spherical aggregations; irregular particles	SEM, AFM	[87]
Atractylodes lancea (Thunb.) DC polysaccharides	Flaky	SEM	[88]
Polygonatum cyrtoneuma hua oligosaccharides	Sheet; snowflake-like nanosheet	SEM, AFM	[89]
Crocus sativus polysaccharides	Scaly structure; island-like structures	SEM, AFM	[90]
Hovenia dulcis polysaccharides	Irregular polymer particle morphology	AFM	[91]
Glehnia littoralis polysaccharides	Spherical; size with 288.4 nm	SEM, DLS	[92]
Chinese yam polysaccharide	Flake structure	SEM	[93]
Codonopsis pilosula polysaccharide	Round conformation	TEM	[94]
Dandelion polysaccharide	Ribbon-shaped	SEM	[95]
Achyranthes bidentata polysaccharide	Irregular sheets	SEM	[96]
Bletilla striata polysaccharide	Flake layer	SEM	[97]
Akebia quinata polysaccharide	Hollow cylinder	SEM	[98]
Ginkgo biloba seed polysaccharides	Spherical structures; geometric shape	SEM	[99]
Angelica sinensis polysaccharide	Spherical structures	SEM, TEM	[100,101]
Large leaf yellow tea polysaccharide	Flaky structure	SEM	[102]

Note: SEM: scanning electron microscope; AFM: atomic force microscopy; DLS: dynamic light scattering; TEM: transmission electron microscope.

3.2. Proteins

Proteins are important biomacromolecules that perform functions vital for sustaining life. Similar to polysaccharides, proteins possess hierarchical structural features, with a primary structure based on amino acid composition and linking sequences, and a tertiary structure based on chain conformation and interactions. Proteins are capable of self-assembling into nanoparticles based on the specific recognition and binding capabilities between proteins or between proteins and other molecules. The self-assembly of proteins leading to the formation of more complex and ordered nanostructures further enriches their *in vivo* functionalities and *in vitro* utilities as drug carriers and biomimetic catalysts. Many proteins from TCM have long been employed to treat various diseases. For example, trichosanthin, extracted from the root tuber of *Trichosanthes kirilowii*, is well known for its immunoregulatory, antitumor, and anti-human immunodeficiency virus (HIV) activities [103]. In addition, other herbal proteins have been found to self-assemble into nanoparticles under certain conditions. For instance, the angelica protein unfolds at high temperatures thereby exposing its hydrophobic sections, which promotes aggregation into angelica protein nanoparticles [104]. The glycyrrhizin-coptis pair has been widely used in clinical practice. Most studies aimed at nanoparticle production have focused on small molecules, such as GA. Li et al. [105] discovered, for the first time, that protein components were present in the precipitate of the licorice-coptis aqueous decoction, which consisted of nanoparticles formed by hydrophobic and electrostatic interactions between the licorice protein and isoquinoline alkaloids in coptis. Compared to monomeric BBR, these nanoparticles showed stronger antibacterial activity. Interestingly, *Pueraria Mirifica* and *Scutellariae* proteins were also found to form nanoparticles during the decoction of *Pueraria Mirifica* and *Scutellariae* [106].

Likewise, structural elucidation of herbal protein-based nanoaggregates is essential for understanding their functions. Camellia seed cake albumin (CSCA) exhibits amphiphilic structural features and excellent water solubility. When combined with chitosan (CS), CSCA/CS complexes are formed owing to electrostatic attraction and hydrophobic interactions. CSCA/CS complexes were further self-assembled into nanoparticles and used for lutein delivery [107]. The morphologies of CSCA/CS and lutein-loaded CSCA/CS nanoparticles were observed using TEM. Both nanoparticles were homogeneous and spherical, with a narrow particle size distribution and rough surfaces. Compared with CSCA/CS nanoparticles, the lutein-loaded CSCA/CS nanoparticles were darker in color, with small aggregates forming on the surface, which could be attributed

to lutein crystals. FT-IR spectroscopy was used to probe intermolecular interactions between lutein, CS, and CSCA molecules. The peak positions in this band of CSCA/CS nanoparticles and lutein-loaded CSCA/CS nanoparticles were blue-shifted, suggesting an increase in hydrogen bonds and the involvement of hydroxyl groups. The amide I and II bands of CS in the spectrum of nanoparticles disappeared, implying the formation of electrostatic interactions between CS and CSCA. Furthermore, the intensities of peaks between wavenumbers ranging from 2800 to 3000 cm^{-1} for CS and CSCA changed following the formation of CSCA/CS nanoparticles, and changed even further after loading with lutein, suggesting the involvement of hydrophobic interactions. More typical examples of nanostructural characterization of proteins from TCM are summarized in Table 3 [108–114].

4. TCM-derived carbon dots

TCM involves methods and techniques aimed at producing preparations according to clinical requirements guided by TCM theory. Some TCM, such as carbonized hair (Xueyutan), *Herba Cirsi Japonici* (Dajitan), and *Rheum Officinale* (Dahuangtan), are generally produced after frying charcoal at high temperatures. Charred TCMs have demonstrated excellent therapeutic efficacy, including hemostasis, hepatoprotection, anti-inflammation, anti-diarrhea, hypoglycemia, and anti-gout effects. The search for a material basis for charred TCM has attracted significant attention in recent years. Nanoparticles from charred TCM are assumed to be inducing their therapeutic effects. These nanoparticles belong to a large family of functional soft nanomaterials termed carbon dots (CDs) [115]. The readers are recommended to refer to several comprehensive reviews regarding the advancement of TCM-derived CDs [116–120]. Herein, we focus on the structural features of CDs, with particular reference to the characterization of their nanostructures.

TCM-derived CDs consist of spherical particles less than 10 nm in diameter. They exhibit good photostability, biocompatibility, low toxicity, and good water dispersibility. Structural characterization of TCM-derived CDs mainly involves morphological observations via TEM, with size being measured using light scattering techniques. Taking Pollen Typhae as an example, Yan et al. [121] prepared novel carbon quantum dots from Pollen Typhae Carbonisata (PTC-CQDs) using a modified pyrolysis method. The samples were calcined in a muffle furnace and ground into a fine powder, following which purified PTC-CQDs were obtained via soaking and water extraction to remove residue and then concentrated and dialyzed. High-performance liquid chromatography measurements confirmed that the small molecules seen in previous extracts were

Table 3
Nanostructural characterization of proteins from traditional Chinese medicine (TCM).

Compounds	Structural features	Characterization techniques	Ref.
Semen Armeniacae Amarum proteins	Spherical; size around 80 nm	TEM, DLS	[108]
English ivy (<i>Hedera helix</i> L.) proteins	Spherical; size of 95.69 ± 5.56 nm	SEM, AFM, DLS	[109]
Radix pseudostellariae protein	Spherical shape	TEM	[110]
Licorice protein	Almost sphere	SEM	[111]
Isatis indigotica Fort. root protein	Spherical	SEM	[112]
Coptidis Rhizoma protein	Irregularly shaped particles	SEM	[113]
Freshwater clam (<i>Corbicula fluminea</i> Muller) soup	Spherical	TEM	[114]

Note: TEM: transmission electron microscope; DLS: dynamic light scattering; SEM: scanning electron microscope; AFM: atomic force microscopy.

absent following the formation of CDs, while TEM indicated that the CQDs were spherical and monodispersed, with a size distribution between 2 and 8 nm. Moreover, high-resolution TEM revealed that the CQDs had a lattice spacing of 0.206 nm. The UV-Vis of the CQDs showed broad absorption centered at 200 nm, but with no significant maximum absorption peaks. FT-IR was used to analyze the CQDs, and several absorption peaks corresponding to characteristic groups were observed at 3419, 2928, 2855, 1634, 1400, 1128 cm^{-1} . These data suggested that interference from small molecules had been eliminated from the CQDs leaving the generated carbon nanodots solely responsible for their medicinal effects. Based on this frame of studying the TCM-derived CDs, many other CQDs were also investigated (Table 4) [122–136]. These studies generated not only new concepts regarding the material basis of TCM-derived CDs, but also new insights into the potential biomedical and healthcare applications of TCM-derived CDs.

5. Challenges and perspectives

The self-assembly of the herbal components of TCM has led to structurally well-defined aggregates, such as micelles, vesicles, hydrogels, or nanoparticles. The discovery of these aggregates offered a new perspective on understanding the efficacy of TCM at the supramolecular aggregate level instead of focusing on the efficacy at the individual biomolecule level. Hence, an unambiguous elucidation of the hierarchical structure, assembly process, and underlying mechanisms of these aggregates may be considered as being essential for subsequent pharmaceutical

research aimed, in particular, at the nanostructure-bioeffect relationship.

At present, the characterization of the morphology of TCM-derived bio-soft matter mainly relies on the exploration of sample characteristics via various electron microscopic techniques (Fig. 8). SEM, which is typically used to observe the surface structure of nanoaggregates, confers the advantages of high magnification, large depth of field, large field of view, and three-dimensional imaging capabilities. However, most TCM-derived bio-soft matter is nonconductive. Hence, the sample must be made conductive via a metal sputtering process prior to observation, to be adapted to the peculiarities in the imaging mechanism (liberated secondary electrons) of SEM. In TEM, the accelerated electrons can pass through the sample, allowing the morphology and crystallization, as well as the internal structure, of the sample to be probed. Modern TEM allows resolutions even below 0.05 nm to be achieved, making it superior to SEM. Nevertheless, preparing a sample with minimal thickness is often necessary to allow electrons to pass through, a process that is more challenging than that involved in SEM. Usually, SEM and TEM are combined to provide complementary structural information regarding aggregates. AFM is another powerful tool that can be used to probe the morphology of nano-aggregates at an atomic-scale resolution. It operates with a distinct imaging mechanism that measures interacting forces between the tip and the atoms on the sample surface, thereby providing information on surface morphology and roughness. AFM provides a true three-dimensional surface map without damaging the sample, which is

Table 4
Characterization of traditional Chinese medicine (TCM)-derived carbon dots.

Compounds	Structural features	Characterization techniques	Ref.
Paeoniae Radix Alba Carbonisata-derived carbon dots (PRAC-CDs)	Nearly spherical; size of 1.0–2.4 nm; diffraction peaks ($2\theta = 21.141^\circ$)	TEM, XRD	[122]
Lonicerae japonicae Flos Carbonisatas- derived carbon dots (LJFC-CDs)	Spherical; size of 1.0–10.0 nm; diffraction peak ($2\theta = 22.765^\circ$)	TEM, XRD	[123]
Radix Sophorae Flavescentis carbonisata-based carbon dots (RSFC-CDs)	Spherical shape; size of 2–3 nm; diffraction peak ($2\theta = 23.7^\circ$)	TEM, XRD	[124]
Armeniacae Semen Amarum Carbonisata-derived carbon dots (ASAC-CDs)	Spherical; diffraction peak ($2\theta = 20.835^\circ$)	TEM, XRD	[125]
Schizonepetae Herba Carbonisata carbon dots (SHC-CDs)	Nearly spherical; size of 0.8–4.0 nm; diffraction peak ($2\theta = 22.8^\circ$)	TEM, XRD	[126]
Moutan cortex carbonisata nano-components (MCC-NCs)	Spherical; size of 0.80–2.8 nm	TEM	[127]
Granati Pericarpium Carbonisatum nano-components (GPC-NCs)	Spherical shape; size of 1.2–2.3 nm; diffraction peak ($2\theta = 6.603^\circ$)	TEM, XRD	[128]
Cirsium setosum Carbonisata carbon dots (CSC-CDs)	Spherical shape	TEM	[129]
Argyi Folium Carbonisata carbon dots (AAFC-CDs)	Spherical; size of 6.0–10.0 nm; diffraction peak ($2\theta = 22.76^\circ$)	TEM, XRD	[130]
Jiaosanxian-derived carbon dots (JSX-CDs)	Spherical; size of 4.4–6.4 nm; diffraction peak ($2\theta = 18.22^\circ$)	TEM, XRD	[131]
Glycyrrhizae Radix et Rhizoma carbon dots (GRR-CDs)	Spherical; size of 1–5 nm; diffraction peak ($2\theta = 23.02^\circ$)	TEM, XRD	[132]
Mulberry silkworm cocoon carbon dots (MSC-CDs)	Spherical; size of 2.26–9.35	TEM	[133]
Puerariae lobatae Radix carbon dots (PLR-CDs)	Spherical; size of 3–10 nm; diffraction peak ($2\theta = 21.3^\circ$)	TEM, XRD	[134]
Aurantii fructus immaturus carbonisata-derived carbon dots (AFIC-CDs).	Spherical; size of 1.1–4.4 nm; diffraction peak ($2\theta = 26.603^\circ$)	TEM, XRD	[135]
Phellodendri Cortex-derived carbon dots (PCC-CDs)	Spherical; size of 1.2–4.8 nm	TEM	[136]

Note: TEM: transmission electron microscope; XRD: X-ray diffraction.

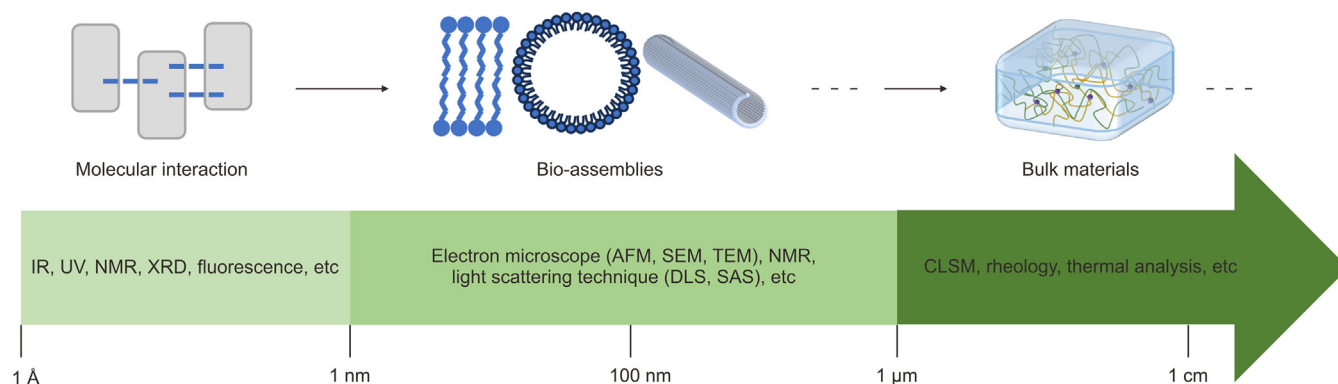


Fig. 8. Hierarchical assembly of bio-constituents from herbal medicines and their structural–ordering characterizations across multi-length scales. IR: infrared; UV: ultraviolet; NMR: nuclear magnetic resonance; XRD: X-ray diffraction; AFM: atomic force microscopy; SEM: scanning electron microscope; TEM: transmission electron microscope; DLS: dynamic light scattering; SAS: small angle scattering; CLSM: confocal laser scanning microscope.

very useful for the conformational characterization of polymers, such as polysaccharides and proteins. Interestingly, a novel methodology involving electrospray mass spectrometry coupled with STM imaging, which was developed recently, allows direct observation of glycans bonded to proteins and lipids at the single-molecule level [137]. Overall, these high-resolution microscopic imaging methods provide precise nanoscale structural information on TCM-derived bio-soft matter systems. However, all samples need to be dried before being visualized for experimental purposes, and thus morphological observations made via such microscopic methods may be affected by artifacts that solely demonstrate the structures in the “dry” state. Small-angle scattering (SAS), which mainly includes SAXS and SANS, may serve as an extremely powerful tool for characterizing nanoscale supramolecular self-assembly systems. One advantage of this technique is the absence of specific requirements for sample preparation. SAXS and SANS can probe samples in many different states (liquids, solids, and soft materials). Hence, SAS may provide intrinsic structural information regarding aggregates in their “wet” state without any artifacts. These advantages of SAS make it particularly suitable for characterizing bio-soft matter systems generated during the processing, and decoction of TCM, irrespective of the sample state.

In addition to establishing the hierarchical structure of TCM-derived bio-soft matter, it is important to focus on another fundamental aspect which involves unveiling the assembly process and underlying mechanisms, which would enable the rational designing and fabrication of certain bio-soft matter as real therapeutics. To this end, it is necessary to gain a proper understanding of how non-covalent interactions, such as H-bonds, π – π interaction, van der Waals forces, and C–H– π interactions, drive the recognition and assembly of molecular building blocks into hierarchal bio-soft matter. Many spectroscopic methods, particularly UV–Vis, fluorescence, FT-IR, and NMR are very useful for probing non-covalent interactions taking place among molecules as well as the binding strengths involved. Additionally, modern advanced synchrotron light source facilities offer opportunities to gain more insight into the assembly process and the mechanisms involved, as well as the hierarchical structure of TCM-derived bio-soft matter, with significantly superior spatiotemporal precision (Fig. 8). In addition to experimental investigations, state-of-the-art computational methodologies, such as the coarse-grain model and the all-atom model in molecular dynamics, are capable of simulating and predicting the evolution of dynamic processes among multiple molecular building blocks with near-perfect precision. For the sake of clarity, we have summarized

the advantages and disadvantages of the abovementioned techniques (Table 5).

The advent and spurt of research on TCM-derived bio-soft matter necessitate the unambiguity in the elucidation of their hierarchical structure, assembly process and mechanism, which is essential to understand their subsequent *in vivo* bioeffects. Currently, most found TCM-derived bio-soft matter is assembled from a single component. And just a few systems are assembled from two components. However, TCM is a well-known multicomponent system, including bioactive small molecules and macromolecules, that treats diseases via multiple pathways and targets. Hence, multicomponent-based and structurally well-defined bio-soft matter systems are expected to be abundant in TCM. The structural hierarchy and multicomponent complexity of these bio-soft matters pose great challenges to unambiguous structural characterization. It is advisable to combine different microscopic and spectroscopic tools to obtain a full structural profile of bio-soft matter in TCM. Intriguingly, computational simulations, such as those of molecular dynamics, may also serve as indispensable tools for modeling the assembly process of multiple molecules and optimizing the eventual structure of bio-soft matter. Artificial intelligence (AI) may offer possible solutions to these challenges. For example, AI algorithms can help analyze spectroscopic data (NMR, FT-IR, mass spectrometry (MS), etc.), leading to the identification and characterization of various compounds present in TCM. AI may also be used to predict dynamic interactions between multiple components and to even model the eventual structures of bio-soft matter assemblies. Compared with the establishment of the hierarchical structure of TCM-derived bio-soft matter *in vitro*, monitoring its *in vivo* circulation and structural evolution may be an even tougher task. This issue is particularly important for elucidating the nanostructure-bioeffect relationship of TCM-derived bio-soft matter at the supramolecular aggregate level. Hence, more advanced *in situ* structural characterization techniques that are designed to analyze living biosystems should be warranted.

The discovery of TCM-derived bio-soft matter has deepened our understanding of what and how the new form of the material basis of TCM executes therapeutic functions. The rapid development of modern physical science and life science, particularly state-of-the-art characterization techniques, has laid a solid foundation for advancing the emerging field of TCM-derived bio-soft matter. In turn, it is assumed that the rise of TCM-derived bio-soft matter will promote interdisciplinary research in physical and life science and also stimulate the development of novel methodologies to disclose the new material basis of TCM featuring multi-component complexity.

Table 5

The advantages and disadvantages of different techniques for characterizing traditional Chinese medicine (TCM)-derived bio-soft matter.

Technology	Advantages	Disadvantages
SEM	High resolution; Large depth of field; Continuously adjustable magnification over a wide range, with sufficient signal brightness in the image even at high magnification; Relative ease of specimen preparation; Dynamic observation is possible.	Less resolution than TEM and AFM, which do not allow observation of molecular and atomic images of substances; Specimens need to be observed in a vacuum environment, limiting the types of samples; Only the surface morphology of the sample can be observed, and structures below the surface cannot be detected; No height orientation information, only two-dimensional planar images; Cannot observe liquid samples.
TEM	Magnification of 10,000× or more; High resolution; Observation of internal structures.	Requires a vacuum environment; May damage samples.
AFM	Providing a three-dimensional surface profile; The sample does not require any processing; The possibility of working in ambient air or even liquid environments; Higher resolution.	Scanning images of a single size; Slow scanning speed; Not suitable for measuring fine distances.
UV-Vis	High sensitivity, low detection limit; High accuracy; The operation is simple, and fast, and the instrument is not complicated; Wide application range; Simultaneous determination of multiple components.	Selectivity is sometimes poor; The analytical components must contain chromophores.
XRD	Crystalline structure determination; Phase analysis; Qualitative and quantitative Analysis; Non-Destructive technique; High resolution.	Complicated sample preparation; Equipment is expensive; Low Sensitivity; Radiation hazard.
DLS	Particle size distribution; High sensitivity; Rapid measurements; Non-invasive technique; Dynamic measurements; Wide applicability.	Size range limitations; Polydispersity challenges; Sample dependent; Sensitivity to aggregation; Limited for low concentrations; Instrumentation complexity.
FT-IR	High speed of analysis; Simplicity of operation; No need for pure samples; Good selectivity; High sensitivity; Less sample damage.	Must have a standard as a reference.
NMR	Non-destructive means of detection; High repeatability; No need for standard samples; Low external influence on results.	Low resolution, not suitable for resolving large molecule structures.
SAXS	Wide range of applications; The possibility of studying the dynamic processes of polymers; The possibility of obtaining statistical averaging information within the specimen; Easy specimen preparation.	Not suitable for three-phase system studies.

Note: SEM: scanning electron microscope; TEM: transmission electron microscope; AFM: atomic force microscopy; UV-Vis: ultraviolet–visible spectroscopy; XRD: X-ray diffraction; DLS: dynamic light scattering; FT-IR: Fourier transform infrared spectrometer; NMR: nuclear magnetic resonance; SAXS: small-angle X-ray scattering.

Declaration of competing interest

The authors declare that there are no conflicts of interest.

CRediT author statement

Guiya Yang: Data curation, Formal analysis, Investigation, Methodology, Visualization, and Writing - Original draft preparation; **Yue Liu:** Data curation, Formal analysis, Investigation, Methodology, Visualization, and Writing - original draft preparation; **Yuying Hu:** Data curation, and Writing - Reviewing and Editing; **Yue Yuan:** Writing - Reviewing and Editing; **Yunan Qin:** Funding acquisition, Validation, and Writing - Reviewing and Editing; **Quan Li:** Conceptualization, Funding acquisition, Investigation, Project administration, Supervision, Validation, Visualization, and Writing - original draft preparation; **Shuangcheng Ma:** Conceptualization, Funding acquisition, Investigation, Project administration, Supervision, Validation, Visualization, and Writing - Original draft preparation.

Acknowledgments

This work was supported by the National Natural Science Foundation of China (Grant No.: 82374033 and 21901067), Ministry of Science and Technology of China (Grant No.: 2023YFC3504100), and Starting Grant from the Ministry of Human Resource and Social Security of China (Quan Li).

References

- [1] Y. Liu, Z. Yang, J. Cheng, et al., Barriers and countermeasures in developing traditional Chinese medicine in Europe, *Front. Med.* 10 (2016) 360–376.
- [2] J. Hou, J. Zhang, C. Yao, et al., Deeper chemical perceptions for better traditional Chinese medicine standards, *Engineering* 5 (2019) 83–97.
- [3] Z. Zhang, T. Bo, Y. Bai, et al., Quadrupole time-of-flight mass spectrometry as a powerful tool for demystifying traditional Chinese medicine, *TRAC* 72 (2015) 169–180.
- [4] Y. Chen, W. Bicker, J. Wu, et al., Ganoderma species discrimination by dual-mode chromatographic fingerprinting: a study on stationary phase effects in hydrophilic interaction chromatography and reduction of sample misclassification rate by additional use of reversed-phase chromatography, *J. Chromatogr., A* 1217 (2010) 1255–1265.

- [5] W.J. Chen, Honoring antiparasitics: The 2015 Nobel Prize in Physiology or Medicine, *Biomed. J.* 39 (2016) 93–97.
- [6] N. Han, X. Huang, X. Tian, et al., Self-assembled nanoparticles of natural phytochemicals (berberine and 3,4,5-Methoxycinnamic acid) originated from traditional Chinese medicine for inhibiting multidrug-resistant *Staphylococcus aureus*, *Curr. Drug Deliv.* 18 (2021) 914–921.
- [7] X. Huang, P. Wang, T. Li, et al., Self-assemblies based on traditional medicine berberine and cinnamic acid for adhesion-induced inhibition multidrug-resistant *Staphylococcus aureus*, *ACS Appl. Mater. Interfaces* 12 (2020) 227–237.
- [8] T. Li, P. Wang, W. Guo, et al., Natural berberine-based Chinese herb medicine assembled nanostructures with modified antibacterial application, *ACS Nano* 13 (2019) 6770–6781.
- [9] X. Tian, P. Wang, T. Li, et al., Self-assembled natural phytochemicals for synergistically antibacterial application from the enlightenment of traditional Chinese medicine combination, *Acta Pharm. Sin.* B 10 (2020) 1784–1795.
- [10] S. Li, Q. Zou, R. Xing, et al., Peptide-modulated self-assembly as a versatile strategy for tumor supramolecular nanotheranostics, *Theranostics* 9 (2019) 3249–3261.
- [11] S. Yadav, A.K. Sharma, P. Kumar, Nanoscale self-assembly for therapeutic delivery, *Front. Bioeng. Biotechnol.* 8 (2020), 127.
- [12] Y. Hou, L. Zou, Q. Li, et al., Supramolecular assemblies based on natural small molecules: union would be effective, *Materials Today Bio* 15 (2022), 100327.
- [13] X. Su, L. Wu, M. Hu, et al., Glycyrrhizic acid: a promising carrier material for anticancer therapy, *Biomed. Pharmacother.* 95 (2017) 670–678.
- [14] F.H. Yang, Q. Zhang, Q.Y. Liang, et al., Bioavailability enhancement of paclitaxel via a novel oral drug delivery system: paclitaxel-loaded glycyrrhizic acid micelles, *Molecules* 20 (2015) 4337–4356.
- [15] R. Yang, X. Zuo, Synchrotron X-ray and neutron diffraction, total scattering, and small-angle scattering techniques for rechargeable battery research, *Small Methods* (2018), 1800064.
- [16] C.J. Gommel, S. Jaksch, H. Frielinghaus, Small-angle scattering for beginners, *J. Appl. Crystallogr.* 54 (2021) 1832–1843.
- [17] D.W.L. Hukins, X-ray Diffraction by Disordered and Ordered Systems, Pergamon, Oxford, 1981.
- [18] L.A. Feigin, D.I. Svergun, Structure Analysis by Small-Angle X-Ray and Neutron Scattering, 1987.
- [19] A. Guinier, G. Fournet, K.L. Yudowitch, Small-Angle Scattering of X-rays, Wiley, New York, 1955.
- [20] K. Matsuoka, R. Miyajima, Y. Ishida, et al., Aggregate formation of glycyrrhizic acid, *Colloids Surf. A Physicochem. Eng. Aspects* 500 (2016) 112–117.
- [21] I.M. Tucker, A. Burley, R.E. Petkova, et al., Adsorption and self-assembly properties of the plant based biosurfactant, glycyrrhizic acid, *J. Colloid Interface Sci.* 598 (2021) 444–454.
- [22] M.V. Zelikman, A.V. Kim, N.N. Medvedev, et al., Structure of dimers of glycyrrhizic acid in water and their complexes with cholesterol: molecular dynamics simulation, *J. Struct. Chem.* 56 (2015) 67–76.
- [23] C. Dargel, R. Geisler, Y. Hannappel, et al., Self-assembly of the bio-surfactant aescin in solution: a small-angle X-ray scattering and fluorescence study, *Colloids Interfaces* 3 (2019), 47.
- [24] I.M. Tucker, A. Burley, R.E. Petkova, et al., Self-assembly of Quillaja saponin mixtures with different conventional synthetic surfactants, *Colloids Surf. A Physicochem. Eng. Aspects* 633 (2022), 127854.
- [25] D.C. Drummond, O. Meyer, K. Hong, et al., Optimizing liposomes for delivery of chemotherapeutic agents to solid tumors, *Pharmacol. Rev.* 51 (1999) 691–743.
- [26] D. Papahadjopoulos, T.M. Allen, A. Gabizon, et al., Sterically stabilized liposomes: improvements in pharmacokinetics and antitumor therapeutic efficacy, *Proc. Natl. Acad. Sci. U. S. A.* 88 (1991) 11460–11464.
- [27] D.-C. Li, X.-K. Zhong, Z.-P. Zeng, et al., Application of targeted drug delivery system in Chinese medicine, *J. Contr. Release* 138 (2009) 103–112.
- [28] K.T. Magar, G.F. Boaf, X. Li, et al., Liposome-based delivery of biological drugs, *Chin. Chem. Lett.* 33 (2022) 587–596.
- [29] M.K. Shanmugam, X. Dai, A.P. Kumar, et al., Ursolic acid in cancer prevention and treatment: molecular targets, pharmacokinetics and clinical studies, *Biochem. Pharmacol.* 85 (2013) 1579–1587.
- [30] X.-H. Wang, S.-Y. Zhou, Z.-Z. Qian, et al., Evaluation of toxicity and single-dose pharmacokinetics of intravenous ursolic acid liposomes in healthy adult volunteers and patients with advanced solid tumors, *Exp. Opin. Drug Metabol. Toxicol.* 9 (2013) 117–125.
- [31] T. Zhao, Y. Liu, Z. Gao, et al., Self-assembly and cytotoxicity study of PEG-modified ursolic acid liposomes, *Mater. Sci. Eng., C* 53 (2015) 196–203.
- [32] J. Wan, Y. Long, S. Liu, et al., Geniposide-loaded liposomes for brain targeting: development, evaluation, and *in vivo* studies, *AAPS PharmSciTech* 22 (2021), 222.
- [33] U. Walthelm, K. Dittrich, G. Gelbrich, et al., Effects of saponins on the water solubility of different model compounds, *Planta Med.* 67 (2001) 49–54.
- [34] H. Kimata, N. Sumida, N. Matsufuji, et al., Interaction of saponin of *Bupleuri radix* with ginseng saponin: solubilization of saikosaponin-a with chikusetsusaponin V (= ginsenoside-Ro), *Chem. Pharm. Bull. (Tokyo)* 33 (1985) 2849–2853.
- [35] X. Dai, X. Shi, Y. Wang, et al., Solubilization of saikosaponin a by ginsenoside Ro biosurfactant in aqueous solution: mesoscopic simulation, *J. Colloid Interface Sci.* 384 (2012) 73–80.
- [36] X.-H. Xu, T.-J. Yuan, H.A. Dad, et al., Plant exosomes as novel nanoplatforms for microRNA transfer stimulate neural differentiation of stem cells *in vitro* and *in vivo*, *Nano Lett.* 21 (2021) 8151–8159.
- [37] C. Dargel, Y. Hannappel, T. Hellweg, Heating-induced DMPC/glycyrhizin bicelle-to-vesicle transition: a X-ray contrast variation study, *Biophys. J.* 118 (2020) 2411–2425.
- [38] L. Fan, B. Zhang, A. Xu, et al., Carrier-free, pure nanodrug formed by the self-assembly of an anticancer drug for cancer immune therapy, *Mol. Pharm.* 15 (2018) 2466–2478.
- [39] J. Wang, W. Qiao, X. Li, et al., A directed co-assembly of herbal small molecules into carrier-free nanodrugs for enhanced synergistic antitumor efficacy, *J. Mater. Chem. B* 9 (2021) 1040–1048.
- [40] X. Du, J. Zhou, J. Shi, et al., Supramolecular hydrogelators and hydrogels: from soft matter to molecular biomaterials, *Chem. Rev.* 115 (2015) 13165–13307.
- [41] P.W. Frederix, G.G. Scott, Y.M. Abul-Haija, et al., Exploring the sequence space for (tri-)peptide self-assembly to design and discover new hydrogels, *Nat. Chem.* 7 (2015) 30–37.
- [42] A.S. Weingarten, R.V. Kazantsev, L.C. Palmer, et al., Supramolecular packing controls H2 photocatalysis in chromophore amphiphile hydrogels, *J. Am. Chem. Soc.* 137 (2015) 15241–15246.
- [43] D. Yuan, X. Du, J. Shi, et al., Mixing biomimetic heterodimers of Nucleopeptides to generate biocompatible and biostable supramolecular hydrogels, *Angew. Chem. Int. Ed.* 54 (2015) 5705–5708.
- [44] N.A. Dudukovic, C.F. Zukoski, Mechanical properties of self-assembled Fmoc-diphenylalanine molecular gels, *Langmuir* 30 (2014) 4493–4500.
- [45] J. Omar, D. Ponsford, C.A. Dreiss, et al., Supramolecular hydrogels: design strategies and contemporary biomedical applications, *Chem. Asian J.* 17 (2022), e202200081.
- [46] J. Raeburn, C. Mendoza-Cuenca, B.N. Cattoz, et al., The effect of solvent choice on the gelation and final hydrogel properties of Fmoc-diphenylalanine, *Matter* 11 (2015) 927–935.
- [47] D. Adams, M.F. Butler, W. Frith, et al., A new method for maintaining homogeneity during liquid-hydrogel transitions using low molecular weight hydrogelators, *Soft Matter* 5 (2009) 1856–1862.
- [48] C. Tang, A.M. Smith, R.F. Collins, et al., Fmoc-diphenylalanine self-assembly mechanism induces apparent pKa shifts, *Langmuir* 25 (2009) 9447–9453.
- [49] Z. Yang, G. Liang, B. Xu, Enzymatic hydrogelation of small molecules, *Acc. Chem. Res.* 41 (2008) 315–326.
- [50] J. Raeburn, A.Z. Zamith Cardoso, D.J. Adams, The importance of the self-assembly process to control mechanical properties of low molecular weight hydrogels, *Chem. Soc. Rev.* 42 (2013) 5143–5156.
- [51] Y. Gao, Y. Dong, Q. Guo, et al., Study on supramolecules in traditional Chinese medicine decoction, *Molecules* 27 (2022), 3268.
- [52] X.-J. Yao, J.-A. Yin, Y.-F. Xia, et al., Puerarin exerts antipyretic effect on lipopolysaccharide-induced fever in rats involving inhibition of pyrogen production from macrophages, *J. Ethnopharmacol.* 141 (2012) 322–330.
- [53] L.-P. Yan, S.-W. Chan, A.S.-C. Chan, et al., Puerarin decreases serum total cholesterol and enhances thoracic aorta endothelial nitric oxide synthase expression in diet-induced hypercholesterolemic rats, *Life Sci.* 79 (2006) 324–330.
- [54] Y. Yuan, J. Zong, H. Zhou, et al., Puerarin attenuates pressure overload-induced cardiac hypertrophy, *J. Cardiol.* 63 (2014) 73–81.
- [55] Y.-X. Zhou, H. Zhang, C. Peng, Puerarin: a review of pharmacological effects, *Phytother. Res.* 28 (2014) 961–975.
- [56] Y. Cai, J. Zhang, Y. He, et al., A supramolecular hydrogel of puerarin, *J. Biomed. Nanotechnol.* 14 (2018) 257–266.
- [57] Z. Pang, Y. Wei, N. Wang, et al., Gel formation of puerarin and mechanistic study during its cooling process, *Int. J. Pharm.* 548 (2018) 625–635.
- [58] Y.H. Feng, X.P. Zhang, Y.Y. Hao, et al., Simulation study of the pH sensitive directed self-assembly of rheins for sustained drug release hydrogel, *Colloids Surf. B Biointerfaces* 195 (2020), 111260.
- [59] J. Zheng, R. Fan, H. Wu, et al., Directed self-assembly of herbal small molecules into sustained release hydrogels for treating neural inflammation, *Nat. Commun.* 10 (2019), 1604.
- [60] W. Zhao, X. Zhang, R. Zhang, et al., Self-assembled herbal medicine encapsulated by an oxidation-sensitive supramolecular hydrogel for chronic wound treatment, *ACS Appl. Mater. Interfaces* 12 (2020) 56898–56907.
- [61] M.P. Peixoto, J. Treter, P.E. de Resende, et al., Wormlike micellar aggregates of saponins from *Ilex paraguariensis* A. St. Hil. (mate): a characterisation by cryo-TEM, rheology, light scattering and small-angle neutron scattering, *J. Pharmaceut. Sci.* 100 (2011) 536–546.
- [62] X. Dai, H. Ding, Q. Yin, et al., Dissipative particle dynamics study on self-assembled platycodin structures: the potential biocarriers for drug delivery, *J. Mol. Graph. Model.* 57 (2015) 20–26.
- [63] H.M. Gu, E. Sun, J. Li, et al., Effect of processing excipient suet oil on formation and absorption of baohuoside I-bile salt self-assembled micelles, *Zhongguo Zhongyao Zazhi* 44 (2019) 5143–5150.
- [64] L.-Y. Shiu, H. Huang, C.Y. Chen, et al., Reparative and toxicity-reducing effects of liposome-encapsulated saikosaponin in mice with liver fibrosis, *Bioscience Reports* 40 (2020), BSR20201219.
- [65] Y. Chen, L.V. Minh, J. Liu, et al., Baicalin loaded in folate-PEG modified liposomes for enhanced stability and tumor targeting, *Colloids Surf. B Biointerfaces* 140 (2016) 74–82.

- [66] M. Zhang, B. Xiao, H. Wang, et al., Edible ginger-derived nano-lipids loaded with doxorubicin as a novel drug-delivery approach for colon cancer therapy, *Mol. Ther.* 24 (2016) 1783–1796.
- [67] Y. Teng, Y. Ren, M. Sayed, et al., Plant-derived exosomal microRNAs shape the gut microbiota, *Cell Host Microbe* 24 (2018) 637–652.e8.
- [68] K. Sundaram, J. Mu, A. Kumar, et al., Garlic exosome-like nanoparticles reverse high-fat diet induced obesity via the gut/brain axis, *Theranostics* 12 (2022) 1220–1246.
- [69] M.K. Sriwastva, Z.B. Deng, B. Wang, et al., Exosome-like nanoparticles from mulberry bark prevent DSS-induced colitis via the AhR/COPS8 pathway, *EMBO Rep.* 23 (2022), e53365.
- [70] B.G. Bag, K. Paul, Vesicular and fibrillar gels by self-assembly of nanosized oleonic acid, *Asian J. Org. Chem.* 1 (2012) 150–154.
- [71] Y. Huang, Y.J. Wang, Y. Wang, et al., Exploring naturally occurring ivy nanoparticles as an alternative biomaterial, *Acta Biomater.* 25 (2015) 268–283.
- [72] Q. Li, Z. Zhang, S.S. Haque, et al., Localized surface plasmon resonance effects by naturally occurring Chinese yam particles, *J. Appl. Phys.* 108 (2010), 123502.
- [73] J. Wang, H. Zhao, K. Zhi, et al., Exploration of the natural active small-molecule drug-loading process and highly efficient synergistic antitumor efficacy, *ACS Appl. Mater. Interfaces* 12 (2020) 6827–6839.
- [74] J. Wang, W. Qiao, H. Zhao, et al., Paclitaxel and betulonic acid synergistically enhance antitumor efficacy by forming co-assembled nanoparticles, *Biochem. Pharmacol.* 182 (2020), 114232.
- [75] J. Cheng, S. Fu, Z. Qin, et al., Self-assembled natural small molecule diterpene acids with favorable anticancer activity and biosafety for synergistically enhanced antitumor chemotherapy, *J. Mater. Chem. B* 9 (2021) 2674–2687.
- [76] A. Saha, J. Adamcik, S. Bolisetty, et al., Fibrillar networks of glycyrrhizic acid for hybrid nanomaterials with catalytic features, *Angew. Chem. Int. Ed. Engl.* 54 (2015) 5408–5412.
- [77] B.G. Bag, S.S. Dash, First self-assembly study of betulonic acid, a renewable nano-sized, 6-6-6-6-5 pentacyclic monohydroxy triterpenic acid, *Nanoscale* 3 (2011) 4564–4566.
- [78] B.G. Bag, S.S. Dash, Hierarchical self-assembly of a renewable nanosized pentacyclic dihydroxy-triterpenoid betulin yielding flower-like architectures, *Langmuir* 31 (2015) 13664–13672.
- [79] K. Zhi, J. Wang, H. Zhao, et al., Self-assembled small molecule natural product gel for drug delivery: a breakthrough in new application of small molecule natural products, *Acta Pharm. Sin. B* 10 (2020) 913–927.
- [80] J. Lu, X. Wu, L. Liu, et al., First Organogelation study of ursolic acid, a natural ursane triterpenoid, *Chem. Lett.* 45 (2016) 860–862.
- [81] Z. Liang, Z. Yin, X. Liu, et al., A glucomannogalactan from *Pleurotus geesteranus*: structural characterization, chain conformation and immunological effect, *Carbohydr. Polym.* 287 (2022), 119346.
- [82] Q. Yuan, J. Zhang, C. Xiao, et al., Structural characterization of a low-molecular-weight polysaccharide from *Angelica pubescens* Maxim. f. *Biserata* Shan et Yuan root and evaluation of its antioxidant activity, *Carbohydr. Polym.* 236 (2020), 116047.
- [83] V.O. Kratky, H. Sembach, Der verknäuelungsgrad von gelöstem cellulosenitrat nach der röntgenkleinwinkelmethode, *Makromol. Chem.* 18 (1956) 463–487.
- [84] T.T. Thanh, V.T. Tran, Y. Yuguchi, et al., Structure of fucoidan from brown seaweed *Turbinaria ornata* as studied by electrospray ionization mass spectrometry (ESIMS) and small angle X-ray scattering (SAXS) techniques, *Mar. Drugs* 11 (2013) 2431–2443.
- [85] Y. Yuguchi, V.T.T. Tran, L.M. Bui, et al., Primary structure, conformation in aqueous solution, and intestinal immunomodulating activity of fucoidan from two brown seaweed species *Sargassum crassifolium* and *Padina australis*, *Carbohydr. Polym.* 147 (2016) 69–78.
- [86] T.T.V. Tran, H.B. Truong, N.H.V. Tran, et al., Structure, conformation in aqueous solution and antimicrobial activity of ulvan extracted from green seaweed *Ulva reticulata*, *Nat. Prod. Res.* 32 (2018) 2291–2296.
- [87] X. Ji, C. Hou, Y. Yan, et al., Comparison of structural characterization and antioxidant activity of polysaccharides from jujube (*Ziziphus jujuba* Mill.) fruit, *Int. J. Biol. Macromol.* 149 (2020) 1008–1018.
- [88] C.-Y. Liu, D.-J. Hu, H. Zhu, et al., Preparation, characterization and immunoregulatory activity of derivatives of polysaccharide from *Actinolydes Lancea* (Thunb.) DC, *Int. J. Biol. Macromol.* 216 (2022) 225–234.
- [89] L. He, B. Yan, C. Yao, et al., Oligosaccharides from *Polygonatum cyrtoneuma* hua: structural characterization and treatment of LPS-induced peritonitis in mice, *Carbohydr. Polym.* 255 (2021), 117392.
- [90] Y. He, H. Peng, H. Zhang, et al., Structural characteristics and immunopotential activity of two polysaccharides from the petal of *Crocus sativus*, *Int. J. Biol. Macromol.* 180 (2021) 129–142.
- [91] B. Yang, Y. Luo, Y. Sang, et al., Isolation, purification, structural characterization, and hypoglycemic activity assessment of polysaccharides from *Hovenia dulcis* (Guai Zao), *Int. J. Biol. Macromol.* 208 (2022) 1106–1115.
- [92] Y. Jing, J. Li, Y. Zhang, et al., Structural characterization and biological activities of a novel polysaccharide from *Glehnia littoralis* and its application in preparation of nano-silver, *Int. J. Biol. Macromol.* 183 (2021) 1317–1326.
- [93] X. Feng, N. Bie, J. Li, et al., Effect of *in vitro* simulated gastrointestinal digestion on the antioxidant activity, molecular weight, and microstructure of polysaccharides from Chinese yam, *Int. J. Biol. Macromol.* 207 (2022) 873–882.
- [94] W. Liu, X. Lv, W. Huang, et al., Characterization and hypoglycemic effect of a neutral polysaccharide extracted from the residue of *Codonopsis pilosula*, *Carbohydr. Polym.* 197 (2018) 215–226.
- [95] L. Lin, Y. Zhu, C. Li, et al., Antibacterial activity of PEO nanofibers incorporating polysaccharide from dandelion and its derivative, *Carbohydr. Polym.* 198 (2018) 225–232.
- [96] Z. Lin, T. Li, Q. Yu, et al., Structural characterization and *in vitro* osteogenic activity of ABPB-4, a heteropolysaccharide from the rhizome of *Achyranthes bidentata*, *Carbohydr. Polym.* 259 (2021), 117553.
- [97] Z. Chen, Y. Zhao, M. Zhang, et al., Structural characterization and antioxidant activity of a new polysaccharide from *Bletilla striata* fibrous roots, *Carbohydr. Polym.* 227 (2020), 115362.
- [98] H. Wang, X. Wang, Y. Li, et al., Structural properties and *in vitro* and *in vivo* immunomodulatory activity of an arabinofuranan from the fruits of *Akebia quinata*, *Carbohydr. Polym.* 256 (2021), 117521.
- [99] J. Hu, Y. Liu, L. Cheng, et al., Comparison in bioactivity and characteristics of Ginkgo biloba seed polysaccharides from four extract pathways, *Int. J. Biol. Macromol.* 159 (2020) 1156–1164.
- [100] Y. Zhang, Z. Cui, H. Mei, et al., Angelica sinensis polysaccharide nanoparticles as a targeted drug delivery system for enhanced therapy of liver cancer, *Carbohydr. Polym.* 219 (2019) 143–154.
- [101] P. Gu, A. Wusiman, S. Wang, et al., Polyethylenimine-coated PLGA nanoparticles-encapsulated *Angelica sinensis* polysaccharide as an adjuvant to enhance immune responses, *Carbohydr. Polym.* 223 (2019), 115128.
- [102] H. Chen, Y. Huang, C. Zhou, et al., Effects of ultrahigh pressure treatment on structure and bioactivity of polysaccharides from large leaf yellow tea, *Food Chem.* 387 (2022), 132862.
- [103] Q. Gong, D. Deng, J. Ding, et al., Trichosanthin, an extract of *Trichosanthes kirilowii*, effectively prevents acute rejection of major histocompatibility complex-mismatched mouse skin allograft, *Transplant. Proc.* 40 (2008) 3714–3718.
- [104] X. Li, Self-assembly Effect of *Angelica Sinensis* Protein and its Application [Master's Thesis], 2018. Fuzhou: Fuzhou University.
- [105] W. Li, Z.-J. Wang, X.-J. Liu, et al., Based on weak bond chemistry, the interaction mechanism between Glycyrrhiza protein and berberine in water decocting process of Rhizomad Coptidis and liquorice was investigated, *Yao Xue Xue Bao* 56 (2021) 2119–2126.
- [106] D. Li, Study on the Proteins Formed by Self-Assembly from Gegen-Qin-Lian Decoction [Master's Thesis], 2013. Fuzhou: Fuzhou University.
- [107] N. Yu, S. Shao, W. Huan, et al., Preparation of novel self-assembled albumin nanoparticles from *Camellia* seed cake waste for lutein delivery, *Food Chem.* 389 (2022), 133032.
- [108] D. Lin, W. Lin, G. Gao, et al., Purification and characterization of the major protein isolated from *Semen Armeniaceae Amarum* and the properties of its thermally induced nanoparticles, *Int. J. Biol. Macromol.* 159 (2020) 850–858.
- [109] S.C. Lenaghan, J.N. Burris, K. Chourey, et al., Isolation and chemical analysis of nanoparticles from English ivy (*Hedera helix* L.), *J. R. Soc. Interface.* 10 (2013), 20130392.
- [110] Q. Weng, X. Cai, F. Zhang, et al., Fabrication of self-assembled *Radix Pseudostellariae* protein nanoparticles and the entrapment of curcumin, *Food Chem.* 274 (2019) 796–802.
- [111] J. Zhou, J. Zhang, G. Gao, et al., Boiling licorice produces self-assembled protein nanoparticles: a novel source of bioactive nanomaterials, *J. Agric. Food Chem.* 67 (2019) 9354–9361.
- [112] J. Zhou, J. Liu, D. Lin, et al., Boiling-induced nanoparticles and their constitutive proteins from *Isatis indigotica* Fort. root decoction: purification and identification, *J. Tradit. Complement. Med.* 7 (2017) 178–187.
- [113] B.-L. Ma, C. Yin, B.-K. Zhang, et al., Naturally occurring proteinaceous nanoparticles in *Coptidis rhizoma* extract act as concentration-dependent carriers that facilitate berberine absorption, *Sci. Rep.* 6 (2016), 20110.
- [114] Z. Yu, G. Gao, H. Wang, et al., Identification of protein-polysaccharide nanoparticles carrying hepatoprotective bioactives in freshwater clam (*Corbicula fluminea* Muller) soup, *Int. J. Biol. Macromol.* 151 (2020) 781–786.
- [115] Y. Zhao, H. Qu, Y. Zhao, Research progress on pharmacological effects of nano-components of charcoal drugs, *Zhongcaoyao* 53 (2020) 921–929.
- [116] Y.-L. Zhang, Y.-L. Wang, K. Yan, et al., Nanostructures in Chinese herbal medicines (CHMs) for potential therapy, *Nanoscale Horiz* 8 (2023) 976–990.
- [117] W.-K. Luo, L.-L. Zhang, Z.-Y. Yang, et al., Herbal medicine derived carbon dots: synthesis and applications in therapeutics, bioimaging and sensing, *J. Nanobiotechnol.* 19 (2021), 320.
- [118] D. Li, K.-Y. Xu, W.-P. Zhao, et al., Chinese medicinal herb-derived carbon dots for common diseases: efficacies and potential mechanisms, *Front. Pharmacol.* 13 (2022) 815479.
- [119] Z. Chen, S.-Y. Ye, Y. Yang, et al., A review on charred traditional Chinese herbs: carbonization to yield a haemostatic effect, *Pharm. Biol.* 57 (2019) 498–506.
- [120] B. Liu, S. Guo, X. Fan, et al., Carbon quantum dot preparation and application to detecting active ingredients in traditional Chinese medicine, *Acupuncture and Herbal Medicine* 1 (2021) 81–89.
- [121] X. Yan, Y. Zhao, J. Luo, et al., Hemostatic bioactivity of novel *Pollen Typhae Carbonisata*-derived carbon quantum dots, *J. Nanobiotechnol.* 15 (2017), 60.
- [122] Y. Zhao, Y. Zhang, H. Kong, et al., Carbon dots from *paenonia radix alba carbonisata*: hepatoprotective effect, *Int. J. Nanomed.* 15 (2020) 9049–9059.

- [123] J. Wu, M. Zhang, J. Cheng, et al., Effect of *Lonicera japonica* Flos Carbonisata-derived carbon dots on rat models of fever and hypothermia induced by lipopolysaccharide, *Int. J. Nanomed.* 15 (2020) 4139–4149.
- [124] J. Hu, J. Luo, M. Zhang, et al., Protective effects of radix *Sophora flavescens* carbonisata-based carbon dots against ethanol-induced acute gastric ulcer in rats: anti-inflammatory and antioxidant activities, *Int. J. Nanomed.* 16 (2021) 2461–2475.
- [125] Y. Zhao, Y. Zhang, H. Kong, et al., Protective effects of carbon dots derived from *Armeniacae Semen Amarum* Carbonisata against acute lung injury induced by lipopolysaccharides in rats, *Int. J. Nanomed.* 17 (2022) 1–14.
- [126] M. Zhang, Y. Zhao, J. Cheng, et al., Novel carbon dots derived from *Schizonepetae Herba* Carbonisata and investigation of their haemostatic efficacy, *Artif. Cells, Nanomed. Biotechnol.* 46 (2018) 1562–1571.
- [127] J. Luo, J. Hu, Y. Liu, et al., The effect of moutan cortex carbonisata nano-components on the blood-cooling and hemostatic, *Acta Pharmacol. Sin.* 56 (2021) 2093–2101.
- [128] Y. Zhao, L. Li, W. Li, et al., Material basis of *Granati Pericarpium* Carbonisatum for antidiarrheal effect from perspective of nanomaterials, *Zhongcaoyao* 52 (2021) 1335–1342.
- [129] J. Luo, M. Zhang, J. Cheng, et al., Hemostatic effect of novel carbon dots derived from *Cirsium setosum* Carbonisata, *RSC Adv.* 8 (2018) 37707–37714.
- [130] H. Kong, Y. Zhao, Y. Zhu, et al., Carbon dots from *Artemisia argyi* folium carbonisata: strengthening the anti-frostbite ability, *Artif. Cells, Nanomed. Biotechnol.* 49 (2021) 11–19.
- [131] Z. Sun, F. Lu, J. Cheng, et al., Hypoglycemic bioactivity of novel eco-friendly carbon dots derived from traditional Chinese medicine, *J. Biomed. Nanotechnol.* 14 (2018) 2146–2155.
- [132] Y. Liu, M. Zhang, J. Cheng, et al., Novel carbon dots derived from *Glycyrrhizae radix et rhizoma* and their anti-gastric ulcer effect, *Molecules* 26 (2021), 1512.
- [133] X. Wang, Y. Zhang, H. Kong, et al., Novel mulberry silkworm cocoon-derived carbon dots and their anti-inflammatory properties, *Artif. Cells, Nanomed. Biotechnol.* 48 (2020) 68–76.
- [134] X. Wang, Y. Zhang, M. Zhang, et al., Novel carbon dots derived from *Puerariae lobatae radix* and their anti-gout effects, *Molecules* 24 (2019), 4152.
- [135] S. Wang, Y. Zhang, H. Kong, et al., Antihyperuricemic and anti-gouty arthritis activities of *Aurantii fructus immaturus* carbonisata-derived carbon dots, *Nanomedicine (Lond.)* 14 (2019) 2925–2939.
- [136] X. Liu, Y. Wang, X. Yan, et al., Novel *Phellodendri cortex* (Huang Bo)-derived carbon dots and their hemostatic effect, *Nanomedicine (Lond.)* 13 (2018) 391–405.
- [137] K. Anggara, L. Sršan, T. Jaroentomeechai, et al., Direct observation of glycans bonded to proteins and lipids at the single-molecule level, *Science* 382 (2023) 219–223.